Mon. Not. R. Astron. Soc. **000**, 1–21 (2012) Printed 24 May 2016 (MN LATEX style file v2.2)

Detection of high Lyman continuum leakage from four low-redshift compact star-forming galaxies

Y. I. Izotov[1],⋆ D. Schaerer[2,3], T. X. Thuan[4], G. Worseck[5], N. G. Guseva[1], I. Orlitová[6] & A. Verhamme[2]

[1]*Main Astronomical Observatory, Ukrainian National Academy of Sciences, 27 Zabolotnoho str., Kyiv 03680, Ukraine*
[2]*Observatoire de Genève, Université de Genève, 51 Ch. des Maillettes, 1290, Versoix, Switzerland*
[3]*IRAP/CNRS, 14, Av. E. Belin, 31400 Toulouse, France*
[4]*Astronomy Department, University of Virginia, P.O. Box 400325, Charlottesville, VA 22904-4325, USA*
[5]*Max-Planck-Institut für Astronomie, Königstuhl 17, 69117 Heidelberg, Germany*
[6]*Astronomical Institute, Czech Academy of Sciences, Boční II 1401, 141 00, Prague, Czech Republic*

arXiv:1605.05160v2 [astro-ph.GA] 21 May 2016

Accepted XXX. Received YYY; in original form ZZZ

ABSTRACT

Following our first detection reported in Izotov et al. (2016), we present the detection of Lyman continuum (LyC) radiation of four other compact star-forming galaxies observed with the Cosmic Origins Spectrograph (COS) onboard the *Hubble Space Telescope* (*HST*). These galaxies, at redshifts of $z \sim 0.3$, are characterized by high emission-line flux ratios [O III]λ5007/[O II]λ3727 $\gtrsim 5$. The escape fractions of the LyC radiation $f_{\rm esc}$(LyC) in these galaxies are in the range of ~ 6 % – 13 %, the highest values found so far in low-redshift star-forming galaxies. Narrow double-peaked Lyα emission lines are detected in the spectra of all four galaxies, compatible with predictions for Lyman continuum leakers. We find escape fractions of Lyα, $f_{\rm esc}$(Lyα) $\sim$ 20% – 40%, among the highest known for Lyα emitters (LAEs). Surface brightness profiles produced from the COS acquisition images reveal bright star-forming regions in the center and exponential discs in the outskirts with disc scale lengths α in the range ~ 0.6 – 1.4 kpc. Our galaxies are characterized by low metallicity, $\sim 1/8 - 1/5$ solar, low stellar mass $\sim$ (0.2 - 4) $\times 10^9$ M$_\odot$, high star formation rates SFR ~ 14 – 36 M$_\odot$ yr^{-1}, and high SFR densities $\Sigma \sim 2$ – 35 M$_\odot$ yr^{-1} kpc^{-2}. These properties are comparable to those of high-redshift star-forming galaxies. Finally, our observations, combined with our first detection reported in Izotov et al. (2016), reveal that a selection for compact star-forming galaxies showing high [O III]λ5007/[O II]λ3727 ratios appears to pick up very efficiently sources with escaping Lyman continuum radiation: all five of our selected galaxies are LyC leakers.

Key words: cosmology: dark ages, reionization, first stars — galaxies: abundances — galaxies: dwarf — galaxies: fundamental parameters — galaxies: ISM — galaxies: starburst

1 INTRODUCTION

One of the key questions in observational cosmology is the identification of the sources responsible for ionization of the Universe after the cosmic Dark Ages, when the baryonic matter was neutral. Quasars ionize their surroundings, but are generally thought to be too rare to have contributed significantly to cosmic reionization (Fontanot, Cristiani & Vanzella 2012). However, a new population of high-redshift, faint AGN candidates has recently been discovered (Giallongo et al. 2015), which, if confirmed, could have played an important role (Madau & Haardt 2015). The more commonly accepted picture is that galaxies are the main contributors to reionization, although the currently identified sources are insufficient to fully ionize the Universe by redshift $z \sim 6$ (Steidel, Pettini & Adelberger 2001; Cowie, Barger & Trouille 2009; Iwata et al. 2009; Robertson et al. 2013). Fainter, low-mass star-forming galaxies (SFGs) below the current detection limit of observations are thought to be responsible for the bulk of the ionizing radiation, since the observed UV luminosity function is very steep at high-z and hence faint galaxies are very numerous (Ouchi et al. 2009; Wise & Chen 2009; Mitra, Ferrara & Choudhury 2013; Yajima, Choi & Nagamine 2011; Bouwens et al. 2015a).

⋆ E-mail: izotov@mao.kiev.ua

© 2012 RAS

For galaxies to reionize the Universe, the escape fraction of their ionizing radiation has to be high enough, typically of the order of 10–20 % (e.g. Robertson et al. 2013, 2015). For example, Dressler et al. (2015) concluded that dwarf galaxies should provide, to the limit of their observations with UV absolute magnitude $M_{\rm UV} \sim -16$ mag, more than 20% of the flux necessary to maintain ionization at $z = 5.7$. Ouchi et al. (2009) have estimated a minimum escape fraction of the LyC radiation $f_{\rm esc}({\rm LyC}) > 0.2$ required to maintain the Universe ionized at $z = 7$. On the other hand, Finkelstein et al. (2012, 2015) estimated $f_{\rm esc}({\rm LyC}) < 13$ % at z =6 if the luminosity function of galaxies extends to $M_{\rm UV} \sim -13$. Others have examined the required average escape fraction from radiative transfer models. For example, Khaire et al. (2016) have calculated that a constant $f_{\rm esc}$(LyC) of 14–22 % is sufficient to reionize the Universe at $z > 5.5$. At $z < 3.5$ they find that $f_{\rm esc}$(LyC) can have values from 0 to 5 %. However, a steep rise in $f_{\rm esc}$(LyC), of at least a factor of $\sim$ 3, is required between $z = 3.5$ and 5.5, according to Khaire et al. (2016). Other studies argue for a slower increase of the escape fraction with redshift (e.g. Haardt & Madau 2012). They model an increase based on available measurements (cited below in the text). So far, there is no physical explanation for an evolving escape fraction.

Although predicting the Lyman continuum escape fraction from galaxies *ab initio* is very challenging, numerous simulations have tried to address this question, sometimes with contrasting results. For example, radiative hydrodynamical simulations of galaxies at the epoch of cosmic reionization predict that the least massive galaxies have the highest $f_{\rm esc}$(LyC) (e.g Razoumov & Sommer-Larsen 2010; Yajima et al. 2011; Wise et al. 2014), while other studies find relatively low escape fractions, $f_{\rm esc}({\rm LyC}) \approx 5$ %, with no strong dependence on galaxy mass and cosmic time (cf. Yajima et al. 2014; Ma et al. 2015), or a declining escape fraction with decreasing galaxy mass (Gnedin, Kravtsov & Chen 2008). According to Kimm & Cen (2014) and Trebitsch, Blaizot & Rosdahl (2015) simulations, the escape fraction of ionizing photons from low-mass galaxies is probably also strongly variable with time, due to the very bursty star formation histories in their low mass halos. Stochastic escape from higher mass galaxies may also be expected (Paardekooper, Khochfar & Dalla Vecchia 2015; Ma et al. 2015).

A different approach has recently been taken by Sharma et al. (2016), who considered a scenario in which ionizing photons escape from regions with a high surface density Σ of the star formation rate (SFR) as suggested by some observations (Heckman et al. 2011; Borthakur et al. 2014). They found that the fraction of the escaping ionizing radiation increases with redshift, reaching values of 5 % – 20 % at $z >$ 6, with the brighter galaxies having higher escape fractions. Clearly, no consensus has been reached on this issue, and empirical data is needed.

Overall, searches for Lyman continuum leakers, both at high and low redshifts, have so far been difficult and largely unsuccessful. Over the past, deep imaging studies at $z \sim 3$ have produced several candidate leaking galaxies (e.g. Steidel et al. 2001; Iwata et al. 2009; Nestor et al. 2011; Mostardi et al. 2013), whereas other teams have only obtained stringent upper limits (e.g. Vanzella et al. 2010a; Boutsia et al. 2011). Vanzella et al. (2010b) has argued quite convincingly that most of the LyC leaking candidates identified from imaging are explained by UV flux contamination by low-z interlopers along the lines of sight of the high-z galaxies. Recent *Hubble Space Telescope* (*HST*) imaging from several groups appear to confirm this explanation, finding e.g. only one robust LyC detection from a sample of 21 candidates (Siana et al. 2015; Mostardi et al. 2015). Currently, the most reliable Lyman continuum leaker detected at high redshift ($z = 3.212$) is the object *Ion2* by Vanzella et al. (2015) from deep imaging. It is confirmed and analyzed in detail by de Barros et al. (2016). *Ion2* shows a high relative escape fraction $f_{\rm esc}^{\rm rel}({\rm LyC}) = 0.64^{+1.1}_{-0.1}$ and shares many properties with the Lyman continuum sources presented in this paper.

From the non-detections at high redshift, there are many empirical determinations of the upper limit of $f_{\rm esc}$(LyC) in the literature. For example, Rutkowski et al. (2016) measured upper limits of $f_{\rm esc}({\rm LyC}) < 9.6$ % from a sample of SFGs at $z \sim 1$ selected to have Hα equivalent widths EW(Hα) > 200Å, which are thought to be close analogs to the sources of reionization. Sandberg et al. (2015) put a 5σ upper limit on the average $f_{\rm esc}$(LyC) of < 24 % for Hα-emitting galaxies at $z = 2.2$. Grazian et al. (2016) found a low limit of < 2 % for SFGs at $z = 3.3$. Bouwens et al. (2015a,b) have shown that $f_{\rm esc}$(LyC) cannot be in excess of 13% in galaxies at $z = 4 - 5$. For the galaxies with $z > 3.06$ Siana et al. (2015) derived strong 1σ limits on the relative escape fraction $f_{\rm esc}^{\rm rel}$(LyC) between 7 % and 9 %, while Vanzella et al. (2010a) obtained an upper limit $f_{\rm esc}$(LyC) in the range 5 % – 20 %.

Since direct observations of high-redshift galaxies are difficult because of their faintness, contamination by lower-redshift interlopers, and the increase of intergalactic medium (IGM) opacity (e.g., Vanzella et al. 2010a, 2012; Inoue et al. 2014; Grazian et al. 2016), one possible approach to bypass these difficulties is to identify local proxies of this galaxy population. However, starburst galaxies at low redshifts are generally opaque to their ionizing radiation (Leitherer et al. 1995; Deharveng et al. 2001; Grimes et al. 2009). This radiation with small escape fractions $f_{\rm esc}$(LyC) of $\sim$1 – 4.5 % is directly detected only in four low-redshift galaxies. Two of these galaxies were observed with the *HST*/COS (Borthakur et al. 2014; Leitherer et al. 2016), one galaxy with the *Far Ultraviolet Spectroscopic Explorer* (*FUSE*) (Leitet et al. 2013) and one galaxy with both the *HST*/COS and *FUSE* (Leitet et al. 2013; Leitherer et al. 2016). We note that *FUSE* suffered from systematic errors for faint objects with flux densities < few times 10^{-15} erg s^{-1} cm^{-2} Å^{-1} as it is seen in Fig. 6 by Fechner & Reimers (2007) and in Fig. 3 by Shull et al. (2010). Knowing that their LyC fluxes are affected by these systematics, Leitet et al. (2013) tried their best to reduce these data. However, the *FUSE* systematics (gain sag and scattered light) were never fully understood or calibrated, so that these challenging measurements might be beyond *FUSE*'s capabilities.

On the other hand, low-mass compact galaxies at low redshifts $z < 1$ with very active star formation may be promising candidates for escaping ionizing radiation (Cardamone et al. 2009; Izotov, Guseva & Thuan 2011; Jaskot & Oey 2013; Stasińska et al. 2015). The general characteristics of these galaxies is the presence of strong emission lines

Table 1. Coordinates, redshifts and O_{32} ratios of selected galaxies

Name	R.A.(2000.0)	Dec.(2000.0)	z	O_{32}[a]
J1152+3400	11:52:04.88	+34:00:49.88	0.3419	5.4
J1333+6246	13:33:03.96	+62:46:03.78	0.3181	4.8
J1442−0209	14:42:31.39	−02:09:52.03	0.2937	6.7
J1503+3644	15:03:42.83	+36:44:50.75	0.3557	4.9

[a]O_{32} = [O III]λ5007/[O II]λ3727.

in the optical spectra of their H II regions powered by numerous O-stars, which produce plenty of ionizing radiation.

Cardamone et al. (2009) used colour-colour diagrams to select a sample of "Green Pea" (GP) compact galaxies from the Sloan Digital Sky Survey (SDSS) named for their green colour. Izotov et al. (2011) instead used not only images but SDSS spectra as well to produce a larger sample of Luminous Compact Galaxies (LCGs) with properties similar to GPs. They have shown that the colour of the compact galaxy with active star formation is determined by the presence of strong emission lines and therefore depends on the galaxy redshift. Therefore, the GPs selected by Cardamone et al. (2009) constitute a subsample of LCGs in a restricted redshift range of $\sim 0.13 - 0.3$, while in general LCGs may have any colour.

In general LCGs and GPs are low-mass and low-metallicity galaxies (Izotov et al. 2014a,b, 2015). Their stellar masses, SFRs and metallicities are similar to those of high-redshift Lyman-alpha emitting (LAE) and Lyman-break galaxies (LBG) (Izotov et al. 2015). Many LCGs and GPs are characterised by high line ratios [O III]λ5007/[O II]λ3727 $\gtrsim 5$ (hereafter O_{32}), reaching values of up to 60 in some galaxies (Stasińska et al. 2015). Such high values may indicate that H II regions are density-bounded allowing escape of ionizing radiation to the IGM, as suggested e.g. by Jaskot & Oey (2013) and Nakajima & Ouchi (2014).

Based on these unique properties of LCGs and GPs, we have selected a sample of five galaxies for spectroscopic observations with the *HST*, in conjunction with the Cosmic Origins Spectrograph (COS). Our aim is to detect escaping ionizing radiation shortward of the Lyman continuum limit at rest wavelengths $\lesssim$ 912Å and the Lyα emission line in these galaxies. Results for the first object, J0925+1403, have been presented by Izotov et al. (2016) who found a high escape fraction $f_{\rm esc}$(LyC) = (7.8 ± 1.1) % and detected a strong double-peaked Lyα emission line, indicating the high escape fraction $f_{\rm esc}$(Lyα) of the radiation in this line.

In this paper we present the results of the *HST*/COS observations for the remaining four galaxies. The selection criteria are discussed in Section 2. The *HST* observations and data reduction are described in Section 3. Extinction in the optical range and element abundances are discussed in Section 4. Global characteristics of the galaxies are derived in Section 5. We derive surface brightness profiles in the near-ultraviolet (NUV) range in Section 6. The reddening law in the UV range is discussed in Section 7. Lyα emission is considered in Section 8. The Lyman continuum detection and the corresponding escape fractions are presented in Section 9. Finally, we briefly discuss our results in Section 10 and summarize the main findings of the paper in Section 11.

2 THE SAMPLE OF COMPACT STAR-FORMING GALAXIES AND SELECTION OF TARGETS FOR *HST* OBSERVATIONS

The spectroscopic data base of the SDSS Data Release 10 (DR10) (Ahn et al. 2014) was used to select a sample of compact SFGs applying the following selection criteria (Izotov et al. 2015): 1) the angular galaxy radius on the SDSS images $R_{50} \leqslant 3''$, where R_{50} is the galaxy's Petrosian radius within which 50% of the galaxy's flux in the SDSS r band is contained; 2) spiral galaxies were excluded; 3) the emission-line ratio [O III]λ4959/Hβ is $\geqslant 1$ to include only galaxies with high-excitation H II regions; 4) galaxies with AGN activity were excluded using line ratios. It was shown by Izotov et al. (2015) that these low-redshift compact SFGs obey similar mass-metallicity, luminosity-metallicity and mass-SFR relations as SFGs at higher redshifts ($z \sim 2 - 5$).

Additional selection criteria were applied for the *HST* observations (Izotov et al. 2016): 1) a high equivalent width EW(Hβ) > 100Å of the Hβ emission line in the SDSS spectrum; this ensures numerous hot O stars producing ionizing LyC radiation; 2) a sufficiently high brightness in the far-ultraviolet (FUV) and a high enough redshift ($z \gtrsim 0.3$) to allow direct LyC observations with the COS; and 3) a high O_{32} ratio $\gtrsim 5$[1], which may indicate the presence of density-bounded H II regions.

The five brightest galaxies in the FUV were selected for *HST*/COS observations. Three of them were selected from the SDSS DR7 and two from the SDSS DR10. The data for the galaxy J0925+1403 have been presented in Izotov et al. (2016). The coordinates, redshifts, and O_{32} ratios of the remaining four galaxies and their apparent magnitudes are shown in Tables 1 and 2, respectively. Their SDSS images are presented in Fig. 1. All galaxies exhibit a very compact structure. Since these LCGs are at redshifts of ~ 0.3, their colours are green on SDSS composite images and thus they can be classified as GP galaxies.

The location of the selected galaxies in the [O III]λ5007/Hβ – [N II]λ6584/Hα diagnostic diagram (Baldwin, Phillips & Terlevich 1981) is shown in Fig. 2. The solid line by Kauffmann et al. (2003) separates SFGs and active galactic nuclei (AGN). The selected galaxies, shown by stars, are located in the SFG region and thus their interstellar medium is ionized by hot stars in the star-forming regions.

We compare the locations in the O_{32} – R_{23} (R_{23}={[O II]3727+[O III]4959+[O III]5007}/Hβ) diagram of the selected galaxies (Fig. 3) with that of high-redshift LAEs that are potentially leaking ionizing radiation (Nakajima & Ouchi 2014), and that of known low-redshift LyC leakers. It is seen that the selected galaxies shown by stars have properties similar to LAEs, implying that they may be good LyC-leaking candidates. This has been confirmed for J0925+1403 with $f_{\rm esc}$(LyC) of ∼8 % (Izotov et al. 2016). On the other hand, the four low-z LyC leakers (Haro 11, Tol 1247−232, J0921+4509 and Mrk 54, Leitet et al. 2013; Borthakur et al. 2014; Leitherer et al. 2016) with the lower $f_{\rm esc}$(LyC) of ∼1–

[1] In this paper, all line ratios are corrected for extinction derived from the Balmer decrement.

Table 2. Apparent magnitudes

Name	SDSS[a]					*GALEX*		*WISE*			
	u	g	r	i	z	FUV	NUV	$W1$	$W2$	$W3$	$W4$
	u(ap)	g(ap)	r(ap)	i(ap)	z(ap)						
J1152+3400	20.43	20.28	19.74	20.63	19.79	20.66	20.38	17.00	15.96	12.65	...
	20.72	20.60	20.06	20.86	20.01						
J1333+6246	20.91	20.76	20.10	20.97	20.27	20.72	20.97	18.14	...	13.28	...
	21.24	21.10	20.48	21.33	20.59						
J1442−0209	20.40	20.30	19.48	20.73	19.77	20.16	20.30	17.14	15.83	11.64	8.29
	20.76	20.61	19.83	21.03	20.01						
J1503+3644	21.00	20.79	20.37	21.11	20.45	21.01	20.76	16.58	15.30	12.31	8.82
	21.37	21.12	20.70	21.46	20.94						

[a] u, g, r, i, z are total modelled SDSS magnitudes. u(ap), g(ap), r(ap), i(ap), z(ap) are magnitudes within the 3″ diameter spectroscopic aperture for J1333+6246 and J1442−0209 and within the 2″ diameter spectroscopic aperture for J1152+3400 and J1503+3644.

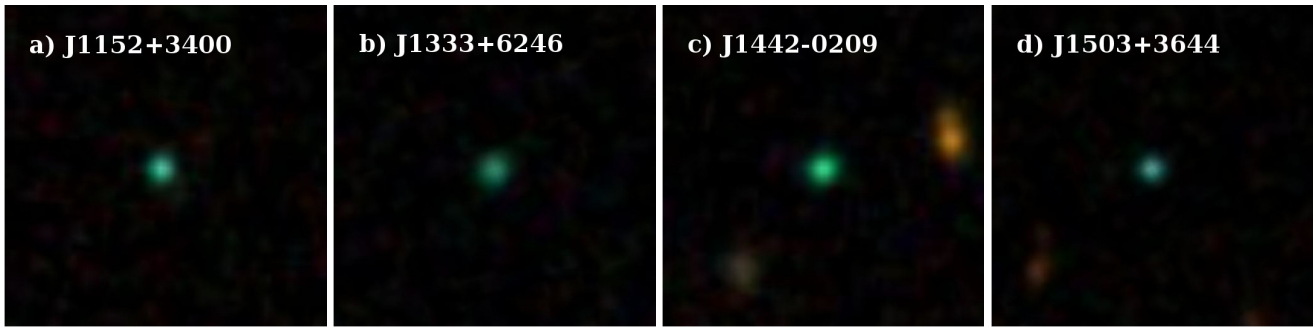

Figure 1. 25″×25″ SDSS composite images of the LyC leaking galaxies.

4.5 % are characterized by lower O_{32} (green filled squares in Fig. 3).

3 *HST*/COS OBSERVATIONS AND DATA REDUCTION

The *HST*/COS (Green et al. 2012) observations were obtained in the course of the program GO13744 (PI: T. X. Thuan). The galaxies were first acquired using COS NUV images with the MIRRORA setting. The galaxy region with the highest number of counts was automatically centered in the 2.″5 diameter spectroscopic aperture (Fig. 4). Although all galaxies show some structure with an extended low-surface-brightness (LSB) component, they are very compact and are localized in the central part of the spectroscopic aperture, which is free of vignetting.

To obtain spectra we used two gratings, G140L and G160M, applying four focal-plane offset positions in each observation to minimize fixed-pattern noise and to patch grid-wire shadows and other detector blemishes (Table 3). The low-resolution G140L grating, with the central wavelength 1280Å for J1152+3400 (same as for J0925+1403, Izotov et al. 2016) and 1105Å for the remaining galaxies, was used to obtain the spectrum, which includes the redshifted LyC emission. The medium-resolution G160M grating with two different central wavelengths was used to obtain spectra with a spectral resolution sufficient to well resolve the redshifted Lyα λ1216 Å line and study its profile.

The data were reduced with custom software specifically designed for faint *HST*/COS targets (Worseck et al. 2011; Syphers et al. 2012). This gives more accurate spectra, improving upon previous results on LyC leakage obtained with the default CALCOS pipeline (Borthakur et al. 2014).

The detector dark current in spectra of the four galaxies, which dominates the COS background, was subtracted in the same way as for J0925+1403, as described in Izotov et al. (2016).

One of us (G. Worseck) investigated the impact of background errors on the determination of the LyC flux. Monte Carlo simulations were run, assuming that the background is a Gaussian variate around the measured value and adopting an estimated uncertainty equal to one standard deviation. In Table 4 we present the measured LyC fluxes with separate statistical and systematic errors (first and second numbers for upper and lower 1σ errors, respectively) for all four galaxies studied in this paper and for J0925+1403 (Izotov et al. 2016). The total counts before background subtraction and the background counts with 1σ uncertainty are also listed in the Table. It is seen that the statistical error by far dominates the systematic error. Due to the large number of counts, the background error does not have a large effect on the result, i.e. the measurements are not background-limited. For J1333+6246 the background-subtracted signal is relatively small ($\sim$ 45 counts), therefore the background uncertainty has a larger impact on the resulting LyC flux. The probabilities that the measured counts are Poisson background fluctuations (i.e. the LyC flux from the galaxy is zero) are 3×10^{-6} for J1333+6246 and $<1\times10^{-6}$ for the other galaxies.

The diagnostic plots of the dark current monitoring pro-

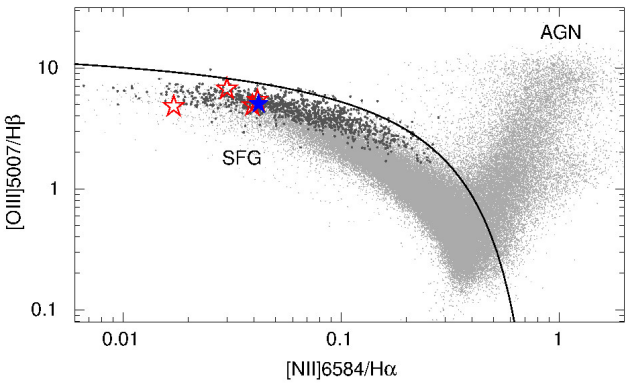

Figure 2. The Baldwin-Phillips-Terlevich (BPT) diagram (Baldwin et al. 1981) for narrow emission-line galaxies. The LyC leaking galaxies (this paper) and J0925+1403 (Izotov et al. 2016) are shown by red open stars and a blue filled star, respectively. The Luminous Compact Galaxies (Izotov et al. 2011) are represented by small dark-grey circles. Also, plotted are the 100,000 emission-line galaxies from SDSS DR7 (cloud of light-grey dots). The solid line by Kauffmann et al. (2003) separates star-forming galaxies (SFG) from active galactic nuclei (AGN).

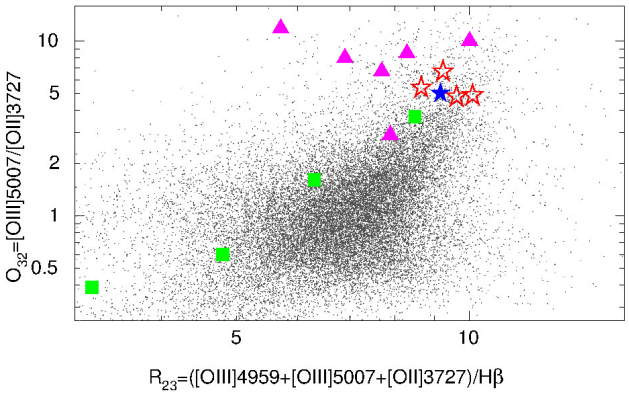

Figure 3. The O_{32} – R_{23} diagram for SFGs. The quantity R_{23} is the total flux of the strongest oxygen lines in the optical spectrum relative to Hβ. This quantity is used for easier comparison with high-redshift LAEs that are potentially leaking ionizing radiation (Nakajima & Ouchi 2014), shown by magenta filled triangles. The location of LyC leaking galaxies corrected for extinction (this paper) and known low-redshift LyC leaking galaxies (Leitet et al. 2013; Borthakur et al. 2014; Leitherer et al. 2016) are shown by red open stars and green filled squares, respectively. The LyC leaking galaxy J0925+1403 (Izotov et al. 2016) is represented by the blue filled star. SDSS SFGs with extinction-corrected line intensities (Izotov et al. 2014a) are shown by grey dots.

Table 3. *HST*/COS observations

Name	Date	Exposure time (s) (Central wavelength (Å))		
		MIRRORA	G140L	G160M
J1152+3400	2015-05-08	558	2655 (1280)	1838,1875 (1600,1623)
J1333+6246	2015-07-06	982	2523 (1105)	1670,1667 (1589,1623)
J1442−0209	2015-07-05	491	2553 (1105)	1887,1890 (1600,1623)
J1503+3644	2015-06-29	808	5753 (1105)	1638,1617 (1600,1623)

Table 4. The observed LyC fluxes and photon counts

Name	Wavelength[a] (Å)	$I_{\rm obs}$(900Å)[b]	Counts Total[c]	Counts Background	Dark rate (s^{-1})
J0925+1403	1120-1180	$2.35^{+0.21+0.00}_{-0.20-0.00}$	425	200.8±5.6	3.5×10^{-6}
J1152+3400	1120-1180	$4.28^{+0.37+0.00}_{-0.34-0.00}$	287	91.2±2.6	3.6×10^{-6}
J1333+6246	1120-1180	$0.83^{+0.21+0.02}_{-0.20-0.02}$	124	79.1±4.4	2.0×10^{-6}
J1442−0209	1120-1178	$1.98^{+0.26+0.01}_{-0.27-0.01}$	192	91.2±3.1	2.8×10^{-6}
J1503+3644	1145-1180	$1.60^{+0.17+0.01}_{-0.16-0.01}$	277	119.8±4.6	2.0×10^{-6}

[a]Wavelength range used for averaging.
[b]in 10^{-17} erg $s^{-1}cm^{-2}Å^{-1}$.
[c]Total count before background subtraction.

grams[2] show that the dark current is correlated with solar activity. The declining radio flux during the year 2015 (all targets were observed between the end of March and the beginning of July 2015) indicates decreasing solar activity. However, the dark rate still exhibits large variations on short timescales, which could be either due to the variable Earth's magnetic field or due to short-time variations in the solar activity that are not tracked well by the solar radio flux measurements.

In the last column of Table 4 we present the dark rates in the LyC regions of our targets which are roughly comparable to the dark rates in the monitoring programs, but differ from them in three aspects: 1). Our dark rates include all pulse heights, whereas the diagnostic plots from the monitoring cut very low and very high pulse heights. 2). Our dark rates are specifically for the LyC region. In particular, our dark is estimated in the spectroscopic aperture, whereas the monitoring plots show the average over the detector which does neither account for gain sag in the aperture, nor local variations in the dark. 3). Our dark rates are estimated from post-processed dark-monitoring data matching the conditions during the observations as closely as possible. A measurement of the true dark rate in the aperture requires post-processing of dark monitoring data. Our estimated uncertainty in the dark varies with the number of dark monitoring exposures matching the observing conditions in a 3-month window around the observation date.

However, the information on the dark variation over timescales of days is not available to us as the dark monitoring is only once per week (exposure 5×1330 s, allocated during Earth occultation). The orbital telemetry data released to the public do not include several quantities that may be helpful for a deeper understanding of the observed dark variations (e.g. magnetic field strength and direction, thermospheric temperature and pressure). In summary, the impact of the dark subtraction will not be large in this study. The time variation and the relatively small intensity of the dark current will not appreciably modify the LyC fluxes quoted here for our objects.

Airglow contamination (N I 1134Å, N I 1200Å, O I 1304Å) was eliminated by considering only data taken in orbital night in the affected wavelength ranges. O I] 1356Å line emission was negligible for all targets except for J1333+6246, for which it was excluded by considering only data taken at Earth limb angles $> 24°$. For J1152+3400, J1333+6246 and J1442−0209, N I 1134Å was considered negligible at all times, but to obtain a conservative flux estimate in the LyC region, we nevertheless substituted the wavelength range 1128 – 1140Å with shadow data. For J1503+3644, the only target with visible N I 1134Å contamination, this was not possible due to detector blemishes falling into the wavelength range of interest during the Earth shadow passage, such that the wavelength range 1128 – 1140Å must be excluded from our analysis. For the targets observed in the 1105Å setup we estimated and subtracted scattered geocoronal Lyα emission following Worseck et al. (2016, in press). The total amount of geocoronal scattered light varies with the specific day and nighttime fractions of the allocated *HST* orbits, contributing a median scattered light flux in LyC range of (1.0 – 2.5) × 10^{-18} erg cm^{-2} s^{-1} $Å^{-1}$. In practice, scattered light was only significant for J1333+6246, which has the lowest LyC flux and the smallest nighttime fraction during the observations (32 %). For J1152+3400, for which geocoronal Lyα was not recorded in the spectrum, we verified that scattered light is negligible in the LyC range by comparing the total spectrum to the one restricted to the night time portion of the orbit. Due to the small circular COS aperture open-shutter background cannot be estimated from the science exposures.

While earthshine and zodiacal light are negligible, Galactic emission has been subtracted considering the exposure-time weighted average flux measured by Murthy (2014) within a radius $r = 2'$ around our targets. The Galactic emission is small, but non-negligible (1 % – 8 % of the measured LyC flux).

4 EXTINCTION IN THE OPTICAL RANGE AND ELEMENT ABUNDANCES

The observed decrement of several hydrogen Balmer emission lines in the SDSS spectra is used to correct the line fluxes for reddening according to Izotov, Thuan & Lipovetsky (1994) and adopting the reddening law by Cardelli, Clayton & Mathis (1989). The correction for the Milky Way and internal extinction was done separately as described in Izotov et al. (2016). The extinction coefficient $C(\rm H\beta)$ derived from the comparison of the observed and theoretical case B hydrogen Balmer decrements corresponds to the extinction $A(\rm H\beta) = 2.512 \times C(\rm H\beta)$ at the Hβ wavelength. To derive the extinction $A(V)$ in the V band Izotov et al. (2016) approximated the ratio $C(\rm H\beta)/A(V)$ as a function of $R(V)=A(V)/E(B-V)$.

[2] http://www.stsci.edu/∼COS/fuv_darks/dark_vs_time_FUVA.png

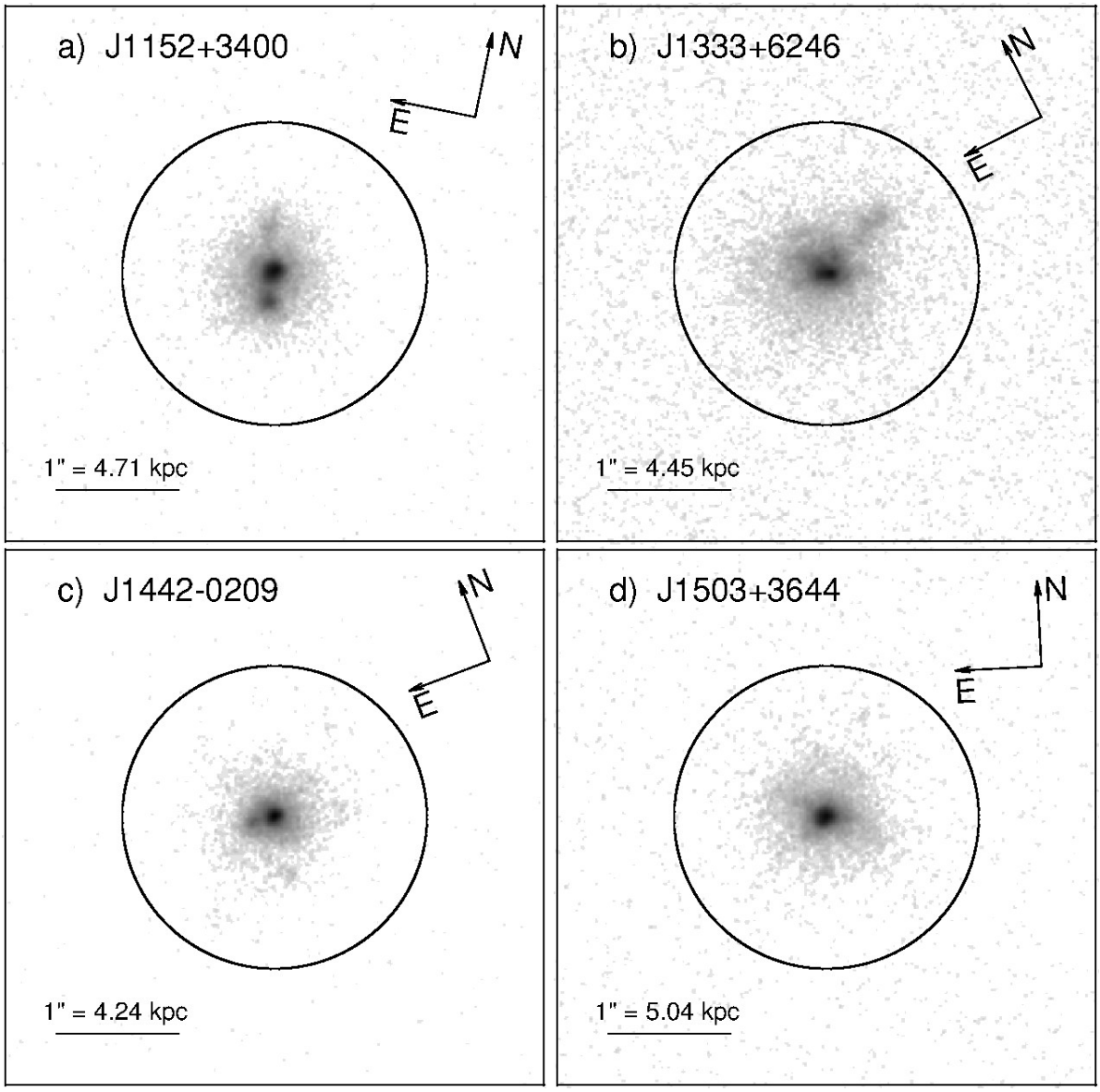

Figure 4. The *HST* COS/NUV acquisition images of the LyC leaking galaxies in log surface brightness scale. The COS spectroscopic aperture with a diameter of 2.″5 is shown by a circle. The linear scale in each panel is derived adopting an angular size distance.

The extinction-corrected emission-line fluxes relative to the Hβ emission line fluxes and the observed equivalent widths are shown in Table 5. The Table also gives the internal extinction coefficients $C(\mathrm{H}\beta)$ and the Hβ emission-line fluxes $I_{\rm cor}(\mathrm{H}\beta)$ corrected for both the Milky Way and internal extinctions.

We use the emission line intensities (Table 5) and the direct $T_{\rm e}$-method to derive electron temperatures and electron number densities, ionic and total element abundances in the interstellar medium (ISM) of the galaxies as described in Izotov et al. (2006). The derived temperatures and element abundances are shown in Table 6. The oxygen abundances of all galaxies are in the narrow range of $\sim 7.8 - 8.0$, i.e. $\sim$1/8 – 1/5 that of the Sun, if the solar abundance of Asplund et al. (2009), 12 + log O/H = 8.69 is adopted. These values are similar to the value of ~ 7.91 found for J0925+1403 (Izotov et al. 2016). The ratios of other element abundances to oxygen abundance are in the range obtained for dwarf emission-line galaxies (e.g. Izotov et al. 2006).

5 GLOBAL PARAMETERS OF THE GALAXIES

We use spectral energy distribution (SED) fits to derive galaxy stellar masses. The fits were performed for the SDSS spectra over the entire observed spectral range of 3900–9200 Å for J1333+6246 and J1442−0209 selected from the SDSS DR7 (same as for J0925+1403, Izotov et al. 2016), and over 3600–10300 Å for J1152+3400 and J1503+3644 selected from the SDSS DR10.

In the galaxies studied here, with rest-frame Hβ equivalent widths EW(Hβ) $\sim 150 - 200$ Å, nebular continuum and line emission are strong and their contributions are removed when determining the stellar mass.

Table 5. Extinction-corrected emission-line fluxes in SDSS spectra

		J1152+3400		J1333+6246		J1442−0209		J1503+3644	
Line	λ[a]	I[b]	EW$_{obs}$[c]	I[b]	EW$_{obs}$[c]	I[b]	EW$_{obs}$[c]	I[b]	EW$_{obs}$[c]
Mg II	2796	13.5±2.2	8	...	...	...	...	33.3±3.8	13
Mg II	2803	7.0±1.9	4	...	...	...	...	19.9±3.0	8
[O II]	3727	105.8±6.1	134	130.2±11.	77	93.6±5.1	117	134.3±8.2	170
H12	3750	5.0±3.4	3	...	...	6.2±2.1	6	4.1±2.3	4
H11	3771	6.0±2.8	4	...	...	5.7±2.1	6	3.7±2.3	3
H10	3798	7.5±2.5	6	...	...	6.2±2.0	7	7.4±2.3	9
H9	3836	8.7±2.3	8	...	...	6.9±2.1	7	9.4±2.3	12
[Ne III]	3869	44.5±3.2	59	52.8±6.1	42	52.2±3.2	69	59.2±4.3	85
H8+He I	3889	20.1±2.5	24	24.2±6.1	17	20.0±2.3	24	20.6±2.7	28
H7+[Ne III]	3969	28.0±2.7	35	33.8±5.8	32	34.3±2.7	50	38.0±3.4	56
Hδ	4101	25.3±2.5	32	27.3±5.7	23	24.9±2.3	40	29.6±2.9	52
Hγ	4340	43.5±3.1	68	47.1±6.3	44	47.7±3.0	94	51.1±3.8	111
[O III]	4363	8.5±1.4	14	17.1±3.7	21	11.3±1.4	23	12.4±1.7	30
He I	4471	4.0±1.1	7	...	...	...	...	4.3±1.3	9
Hβ	4861	100.0±5.5	198	100.0±8.5	194	100.0±5.0	312	100.0±6.0	297
[O III]	4959	189.1±9.3	407	208.7±15.	434	205.7±9.2	494	221.1±12.	544
[O III]	5007	571.1±26.	1230	623.2±41.	1230	624.4±26.	1626	653.8±32.	1403
He I	5876	8.9±1.1	27	9.0±2.5	20	5.5±1.0	20	10.1±1.4	35
[O I]	6300	4.3±0.9	17	7.0±2.1	21	...	...	4.4±0.9	27
[S III]	6312	1.6±0.7	6	...	...	...	...	1.8±0.7	12
Hα	6563	282.2±14.	1320	276.1±21.	817	280.3±13.	1122	280.2±15.	1438
[N II]	6583	11.7±1.2	53	4.7±1.8	21	8.4±1.0	38	11.1±1.4	55
[S II]	6717	11.9±1.3	56	...	...	6.7±1.0	22	10.5±1.3	64
[S II]	6731	10.3±1.2	47	...	...	6.9±1.0	21	8.9±1.2	56
He I	7065	5.0±0.8	29	...	...	...	...	3.6±0.8	20
[Ar III]	7136	6.4±0.9	38	...	...	...	...	5.3±0.9	50
C(Hβ)(int)		0.085		0.070		0.085		0.130	
I_{cor}(Hβ)[d]		30.8		12.2		38.9		27.0	

[a]Rest-frame wavelength in Å.
[b]$I = 100\times I_{cor}(\lambda)/I_{cor}(H\beta)$, where $I_{cor}(\lambda)$ and $I_{cor}(H\beta)$ are emission-line fluxes, corrected for both the Milky Way and internal extinction.
[c]Observed equivalent width in Å.
[d]in 10^{-16} erg s^{-1} cm^{-2}.

To fit the SEDs we carried out a series of Monte Carlo simulations using the technique described e.g. in Guseva et al. (2007), Izotov et al. (2015) and Izotov et al. (2016). The best solutions can be found for different combinations of evolutionary tracks, stellar atmosphere models and initial mass functions. As shown by Izotov et al. (2016), all these solutions provide almost equally good fits at rest-frame wavelengths greater 912Å and show small variations of the LyC. Therefore, in this paper, for the sake of definiteness, we have adopted a Salpeter IMF (Salpeter 1955), Geneva evolutionary tracks (Meynet et al. 1994) of non-rotating stars and a combination of stellar atmosphere models (Lejeune et al. 1997; Schmutz et al. 1992). The optical galaxy spectra with the overlaid stellar (thin green lines), nebular (thin blue lines) and total stellar and nebular (thick red lines) SEDs are shown and labelled in Fig. 5.

The observed fluxes were transformed to luminosities adopting luminosity distances derived with the cosmological calculator (NED, Wright 2006), based on the cosmological parameters H_0=67.1 km s^{-1}Mpc^{-1}, Ω_Λ=0.682, Ω_m=0.318 (Ade et al. 2014). Stellar masses and starburst ages derived from the SED fitting of the SDSS optical spectra are presented in Table 7. We also derived extinction-corrected absolute AB SDSS g-band and *Galaxy Evolution Explorer* (*GALEX*) FUV magnitudes not shown in the Table. They are in the range −20.4 - −21.3 mag, while the magnitudes non-corrected for extinction are $\sim 0.2-0.3$ mag and ~ 1 mag fainter in the g and FUV bands, respectively. We note that the photometric data and UV spectra were not used in the SED fitting, but they are useful for checking the consistency of the SEDs derived from the optical spectra. The derived stellar masses (Table 7) are relatively low, corresponding to that for dwarf galaxies, despite the high brightness due to the active ongoing star formation.

The Hβ luminosity L(Hβ) and SFR were derived from the extinction-corrected Hβ flux. Additionally, they were also corrected for aperture effects using the relation $2.512^{r(ap)-r}$, where r and r(ap) are respectively the SDSS r-band total magnitude and the magnitude within the round spectroscopic 3″ diameter aperture for J1333+6246 and J1442−0209, and within the round spectroscopic 2″ diameter aperture for J1152+3400 and J1503+3644. According to Table 2 the aperture correction factors are $\sim 1.3-1.4$. High Hβ luminosities (Table 8) are produced by the ionizing radiation of a large number of hot massive stars, corresponding to the equivalent numbers of OV7 stars in the range $(1–3)\times10^5$ assuming the number of ionizing photons per O7V star of 1×10^{49} s^{-1} (Leitherer 1990), slightly lower

Table 6. Physical conditions and chemical composition

Galaxy	J1152+3400	J1333+6246	J1442−0209	J1503+3644
T_e ([O III]), K	13430±900	17780±2150	14580±830	14850±950
T_e ([O II]), K	12980±820	15200±1720	13750±730	13910±830
T_e ([S III]), K	12600±750	16320±1790	13480±690	13560±790
N_e ([S II]), cm^{-3}	310±300	100[a]	710±620	280±360
$O^+/H^+\times10^5$	1.60±0.32	1.13±0.34	1.21±0.19	1.59±0.28
$O^{2+}/H^+\times10^5$	8.38±1.59	4.59±1.34	7.35±1.13	7.40±1.27
O/H×10^5	9.98±1.62	5.72±1.38	8.56±1.15	9.00±1.30
12+log O/H	8.00±0.07	7.76±0.11	7.93±0.06	7.95±0.06
$N^+/H^+\times10^6$	1.16±0.17	0.34±0.12	0.74±0.10	0.95±0.14
ICF(N)[b]	5.86	4.86	6.54	5.38
N/H×10^6	6.82±0.11	1.64±0.60	4.86±0.71	5.11±0.79
log N/O	−1.17±0.10	−1.54±0.19	−1.25±0.09	−1.25±0.09
$Ne^{2+}/H^+\times10^5$	1.67±0.35	0.89±0.27	1.52±0.25	1.63±0.30
ICF(Ne)[b]	1.07	1.09	1.06	1.09
Ne/H×10^5	1.79±0.42	0.97±0.33	1.60±0.29	1.77±0.37
log Ne/O	−0.75±0.12	−0.77±0.18	−0.73±0.10	−0.71±0.11
$S^+/H^+\times10^6$	0.29±0.04	...	...	0.22±0.03
$S^{2+}/H^+\times10^6$	1.45±0.68	...	...	1.29±0.54
ICF(S)[b]	1.43	...	...	1.34
S/H×10^6	2.48±0.97	...	...	2.03±0.73
log S/O	−1.60±0.18	...	...	−1.65±0.17
$Ar^{2+}/H^+\times10^7$	3.57±0.63	...	...	2.57±0.49
ICF(Ar)[b]	1.15	...	...	1.14
Ar/H×10^7	4.12±0.72	...	...	2.92±0.56
log Ar/O	−2.38±0.10	...	...	−2.49±0.10

[a]Assumed value.
[b]Ionization correction factor.

Table 7. Global parameters

Name	12+logO/H	D[a] (Mpc)	log $M_\star$[b] (log M$_\odot$)	SB age (Myr)	SFR (M$_\odot$ yr^{-1})	α[c] (kpc)	Σ[d] (M$_\odot$ yr^{-1}kpc^{-2})
J1152+3400	8.00±0.07	1888	9.59	4.1	39	0.59	35.5
J1333+6246	7.76±0.11	1736	8.50	1.6	14	1.44	2.2
J1442−0209	7.93±0.06	1582	8.96	3.4	36	0.86	15.5
J1503+3644	7.95±0.06	1975	8.22	4.0	38	1.34	6.8

[a]Luminosity distance.
[b]$M_\star$ is the stellar mass.
[c]Exponential disc scale length.
[d]$\Sigma = 12.6\ M_\odot\ \mathrm{yr}^{-1}\mathrm{kpc}^{-2}$ for J0925+1403.

than the value of 5×10^5 for J0925+1403. Consequently, the SFRs derived from the Hβ luminosity using the relation by Kennicutt (1998), are also high, 14 – 39 M$_\odot$ yr^{-1}, and similar to $\sim$ 50 M$_\odot$ yr^{-1} in J0925+1403 (Izotov et al. 2016).

6 SURFACE BRIGHTNESS PROFILES IN THE NUV RANGE

We can use the COS/NUV acquisition images of our galaxies to determine their surface brightess (SB) profiles. These images suffer vignetting at radii greater than 0.″5 from the center of the detector. In particular, the throughput at the radius 0.″8 is 0.8 times of that in the center of the aperture[3]. Fortunately, radii of our galaxies are small (Fig. 4). Therefore, to the first order, we may neglect vignetting effects. As two NUV frames were obtained during acquisition, we combine both images. Then, since transmissions of *GALEX*/NUV and COS/MIRRORA are similar[4,5], the images were approximately reduced to the absolute scale using

[3] http://www.stsci.edu/hst/cos/documents/handbooks/current/ch06.COS_Imaging2.html
[4] http://www.stsci.edu/hst/cos/documents/isrs/ISR2010_10.pdf
[5] http://svo2.cab.inta-csic.es/svo/theory/fps3/index.php?id=GALEX/GALEX.NUV&&mode=browse&gname=GALEX&gname2=GALEX#filter

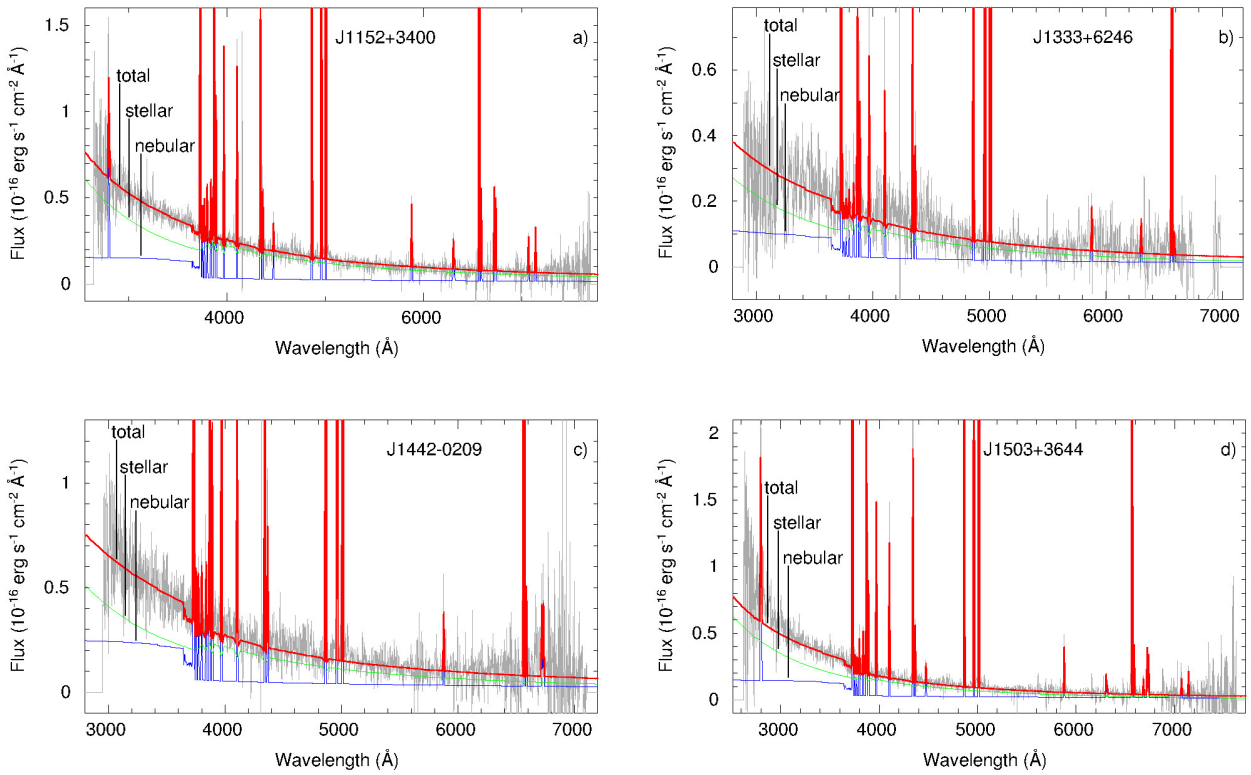

Figure 5. SED fitting of the optical spectra of LyC leaking galaxies. The rest-frame extinction-corrected spectra are shown by grey lines. The stellar, nebular, and total modelled SEDs are shown by thin green, thin blue and thick red lines, respectively, and are labelled.

the total *GALEX* NUV magnitudes (Table 2). Finally, the routine *ellipse* in IRAF[6]/STSDAS[7] was used to produce SB profiles. We derived also the SB profile of J0925+1403 which was not discussed by Izotov et al. (2016). The SB profiles are shown in Fig. 6a-e. The shape of all profiles is very similar, with a sharp SB increase in the central part corresponding to the brightest star-forming region in the center of the galaxy, and a linear SB decrease (in magnitudes) of the extended LSB component in the outward direction.

This linear decrease is characteristic of disc galaxies and can be described by the relation

$$\mu(r) = \mu(0) + 1.086 \times \frac{r}{\alpha}, \quad (1)$$

where μ is the surface brightness, r is the distance from the center, and α is the disc scale length of the outer disc.

The derived scale lengths of $\sim 0.6 - 1.4$ kpc (Table 7) are larger by a factor 2–4 than typical scale lengths of blue compact dwarf (BCD) galaxies which show very similar morphology (e.g. Papaderos et al. 2002). They follow however the $\alpha - M_\star$ relation for the SDSS disc galaxies (Fathi et al. 2010). But we note that the scale lengths for BCDs and SDSS disc galaxies are derived in the optical or near-infrared broad bands. A direct comparison with the scale lengths in the UV range may be somewhat uncertain, as different stellar populations may contribute to the light of the LSB component in the UV and optical ranges.

However, the sizes of our galaxies in the UV can directly be compared with those of galaxies at high redshifts. Curtis-Lake et al. (2016) have shown that half-light radii of $z = 3 - 8$ galaxies are ~ 1 kpc, which are very similar to the scale lengths of our galaxies. The compact morphology and high SFR of our objects imply high SFR densities $\Sigma \sim 2 - 35$ $M_\odot$ yr^{-1} kpc^{-2} (Table 7, Fig. 7), among the highest known (Lehnert & Heckman 1996). Sharma et al. (2016) have argued that galaxies with high Σs may be efficient at letting ionizing radiation escape. High UV luminosities and high SFR densities may result in outflows which produce channels in the neutral gas, allowing ionizing radiation to leak out. However, the data for our galaxies are not sufficient to verify this possibility.

7 REDDENING LAW IN THE UV RANGE

The extinction curve in the optical range is insensitive to variations of $R(V)$. On the other hand, the correction of observed fluxes in the UV range for extinction critically depends on the adopted reddening law, which at low metallicities is steeper than the canonical curve with $R(V) = 3.1$ (Bouchet et al. 1985; Gordon & Clayton 1998; Gordon et al.

[6] IRAF is distributed by the National Optical Astronomy Observatories, which are operated by the Association of Universities for Research in Astronomy, Inc., under cooperative agreement with the National Science Foundation.
[7] STSDAS is product of the Space Telescope Science Institute, which is operated by AURA for NASA.

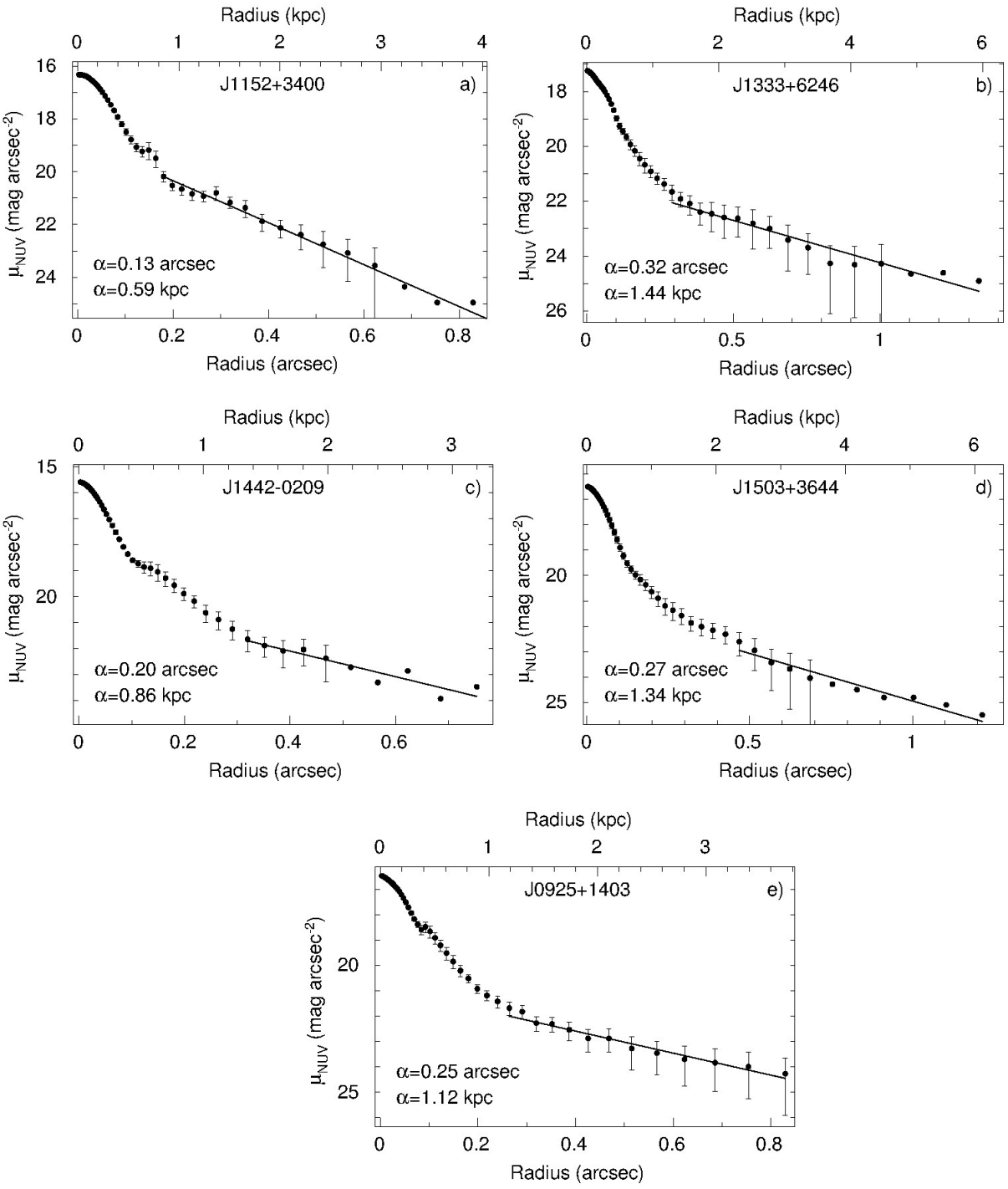

Figure 6. Surface brightness profiles of galaxies derived from the COS/NUV acquisition images. The linear fits are shown for the range of radii used for fitting.

2003). Therefore, we may expect the reddening law in our galaxies to be characterized by $R(V) < 3.1$. To verify that expectation, a comparison of the modelled SEDs with the observed photometric and spectroscopic data in the entire UV and optical range is needed.

The observed UV *HST*/COS and optical SDSS spectra are shown in Fig. 8 by grey lines. Their fluxes are consistent with the SDSS photometric fluxes shown by the orange filled circles. As for *GALEX* UV photometric data (magenta filled squares), they are in agreement with the COS spectra of J1152+3400 and J1503+3644 (and J0925+1403, Izotov et al. 2016), but deviate somewhat in the cases of J1442−0209 and J1333+6246. The deviation is the largest in the FUV band despite the relatively low quoted *GALEX* magnitude errors of 0.05 mag and 0.17 mag for J1442−0209 and J1333+6246, respectively.

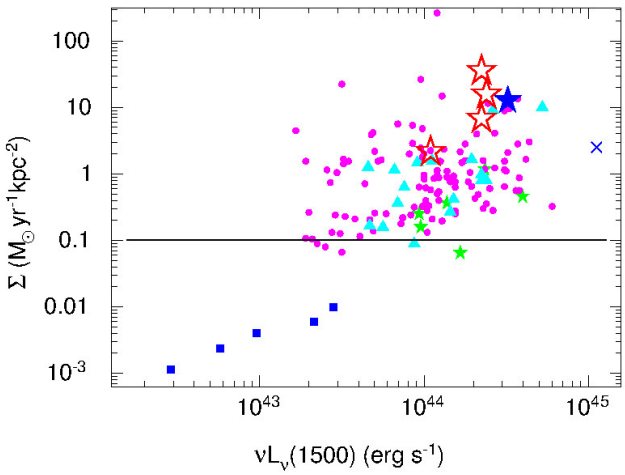

Figure 7. The dependence of the mean surface density of star formation rate Σ on the luminosity $\nu L_\nu(1500)$. The galaxies from this paper are shown by large red open stars and the one from Izotov et al. (2016) by a large blue filled star. These data are corrected for extinction. For comparison, the average data for SDSS galaxies (Brisbin & Harwit 2012) are shown by filled squares, and LBGs at z = 3, 6, and 8 (Curtis-Lake et al. 2016) by small filled stars, circles, and triangles. The cross indicates the location of the Borthakur et al. (2014) galaxy. The horizontal black line shows the critical Σ for outflows (Heckman et al. 2011).

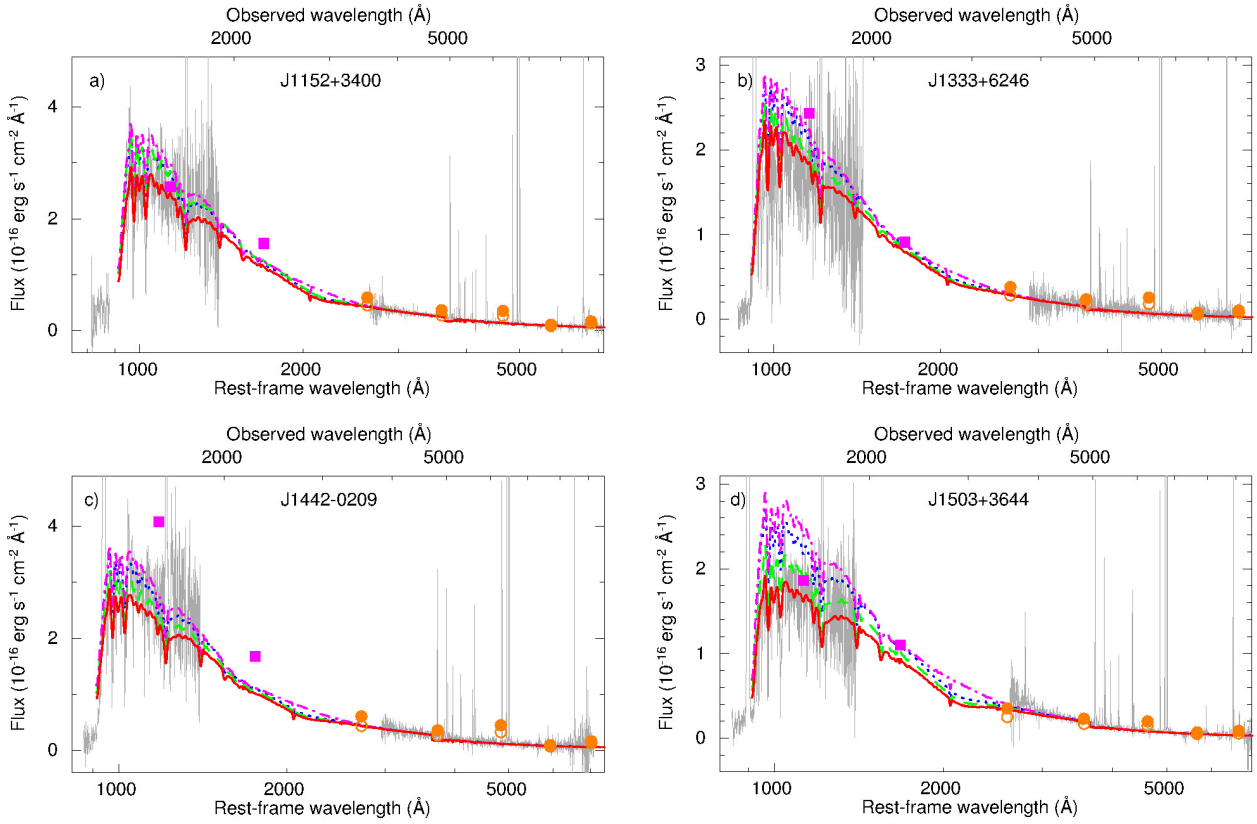

Figure 8. A comparison of the observed UV and optical spectra, and photometric data with the modelled SEDs. The observed spectra are shown by grey lines. The total *GALEX* and SDSS photometric fluxes are represented by magenta filled squares and orange filled circles, respectively, while the SDSS photometric fluxes within a round spectroscopic aperture of 3″ in diameter for J1333+6246 and J1442−0209, and of 2″ in diameter for J1152+3400 and J1503+3644 are shown by open circles. Modelled SEDs, which are reddened by the Milky Way extinction with $R(V)_{\rm MW}$ = 3.1 and internal extinction with $R(V)_{\rm int}$ = 3.1, 2.7, and 2.4 adopting the reddening law by Cardelli et al. (1989) are shown by blue dotted, green dashed and red solid lines, respectively, while modelled SEDs, which reddened by the Milky Way extinction with $R(V)_{\rm MW}$ = 3.1 adopting the reddening law by Cardelli et al. (1989) and internal extinction adopting the reddening law by Calzetti et al. (1994) are represented by magenta dash-dotted lines.

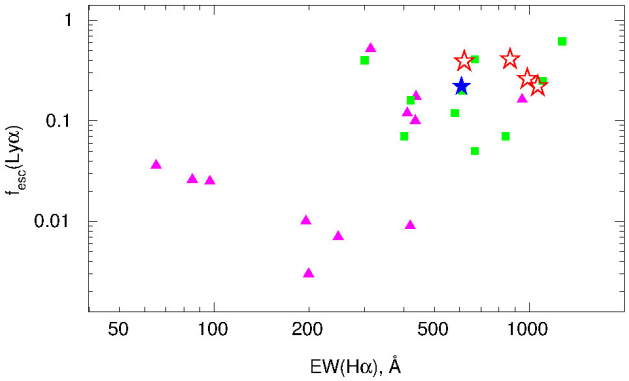

Figure 9. The dependence of the Lyα escape fraction $f_{\rm esc}$(Lyα) on the rest-frame equivalent width EW(Hα) of the Hα emission line. Galaxies from this paper and from Izotov et al. (2016) are represented by red open stars and a blue filled star, respectively. For comparison are shown the GPs studied by Henry et al. (2015) (green filled squares), and nearby galaxies from the Lyman Alpha Reference Sample (LARS) of Östlin et al. (2014) and Hayes et al. (2014) (magenta filled triangles).

To compare with the observed spectra, we reddened the intrinsic modelled SEDs in the optical range and their extrapolations in the UV range, adopting $R(V)_{\rm MW} = 3.1$ for the Milky Way extinction, and $R(V)_{\rm int} = 3.1$ (blue dotted lines), 2.7 (green dashed lines) and 2.4 (red solid lines) for the internal extinction. As before, the Milky Way extinction was applied to SEDs redshifted to the observed wavelengths and the internal extinction to spectra at rest-frame wavelengths. We adopted the reddening curve by Cardelli et al. (1989) parameterized by the corresponding values of $R(V)_{\rm MW}$ and $R(V)_{\rm int}$, except for $\lambda = 912 - 1250$ Å, where the reddening curve of Mathis (1990) with the respective $R(V)$'s is used. The reddening curve at $\lambda < 912$ Å is also provided by Mathis (1990), but it may be somewhat uncertain. Fortunately, these uncertainties do not influence the values of the LyC escape fractions discussed below, which are determined by the observed to intrinsic flux ratios. The only reddening correction needed in the UV is for the observed LyC flux of the Milky Way in the observed wavelength range 1140-1180 Å, where the reddening law is more reliable.

It is seen that the SEDs reddened with $R(V)_{\rm int} = 3.1$ do not fit the observed fluxes in the UV range. A higher extinction coefficient is needed in the UV. On the other hand, a SED reddened by the same extinctions $A(V)_{\rm MW}$ and $A(V)_{\rm int}$, but with $R(V)_{\rm int} = 2.4$, nicely reproduces the observed fluxes, with the exception of J1442−0209, for which $R(V)_{\rm int} = 2.7$ is more appropriate.

A similar conclusion has been drawn by Izotov et al. (2016) for J0925+1403. It appears that a $R(V)_{\rm int}$ with a value lower than the canonical one of 3.1 is more appropriate for dwarf galaxies with low metallicities.

Calzetti, Kinney & Storchi-Bergmann (1994) and Calzetti et al. (2000) analyzed the SEDs in the UV range of star-forming galaxies and found that star formation occurs in dusty regions. They proposed a reddening curve for star-forming galaxies that is less steep than the one for the Milky Way and Magellanic Clouds. If this curve was to be applied to our GP galaxies, together with the $A(V)_{\rm int}$ derived from the optical spectrum, the reddened modelled SED would lie above the observed COS UV spectrum (magenta dash-dotted lines in Fig. 8). Thus to fit the observed optical and UV spectra, the Calzetti reddening law would require a higher extinction in the UV range than that determined from the Balmer decrement.

We note that the galaxies used by Calzetti et al. (1994) and Calzetti et al. (2000) for the reddening curve determination have properties that are quite different from ours. In particular, the excitation of the H II regions in our galaxies, as characterized by the O_{32} ratio, is considerably higher. Thus, the Calzetti et al. (1994) reddening law, determined for dustier and more metal-rich galaxies, may not be applied to our five galaxies with low metallicities and extinctions if the same extinction $A(V)_{\rm int}$ is adopted for the UV and optical ranges.

8 LYα EMISSION

Strong Lyα λ1216 Å emission lines are detected in the medium-resolution spectra of all galaxies obtained with the G160M grating. Their profiles show two peaks with a small separation between the blue and red peaks, similar to profiles observed in some other GP galaxies (Jaskot & Oey 2013; Henry et al. 2015; Izotov et al. 2016; Yang et al. 2016). Correcting for the Milky Way reddening, we obtain the Lyα flux densities presented in Table 8. We find that the extinction-corrected luminosities L(Lyα) and rest-frame equivalent widths EW(Lα) of the Lyα line are among the highest known for both low- and high-redshift Lyα emitters (Table 8).

Comparing the extinction-corrected Lyα/Hβ flux ratios and the case B flux ratio of 23.3 for an electron temperature $T_{\rm e} = 10000$K and an electron number density $N_{\rm e} = 100$ cm^{-3} (Hummer & Storey 1987; Storey & Hummer 1995), we find that the Lyα escape fractions are in the range $\sim 20 - 40$ %, among the highest known so far for GP galaxies (Fig. 9, Henry et al. 2015; Hayes 2015). These high escape fractions are consistent with a low H I column density, and the very young age of the starbursts in our galaxies, as evidenced by their high EW(Hβ)s. A similar high value of $f_{\rm esc}$(Lyα) was obtained for J0925+1403 (Izotov et al. 2016).

The double-peaked Lyα line profile of J0925+1403 was briefly discussed in Izotov et al. (2016). The Lyα line profiles for the entire sample will be shown and analyzed in a separate paper (Verhamme et al., in preparation).

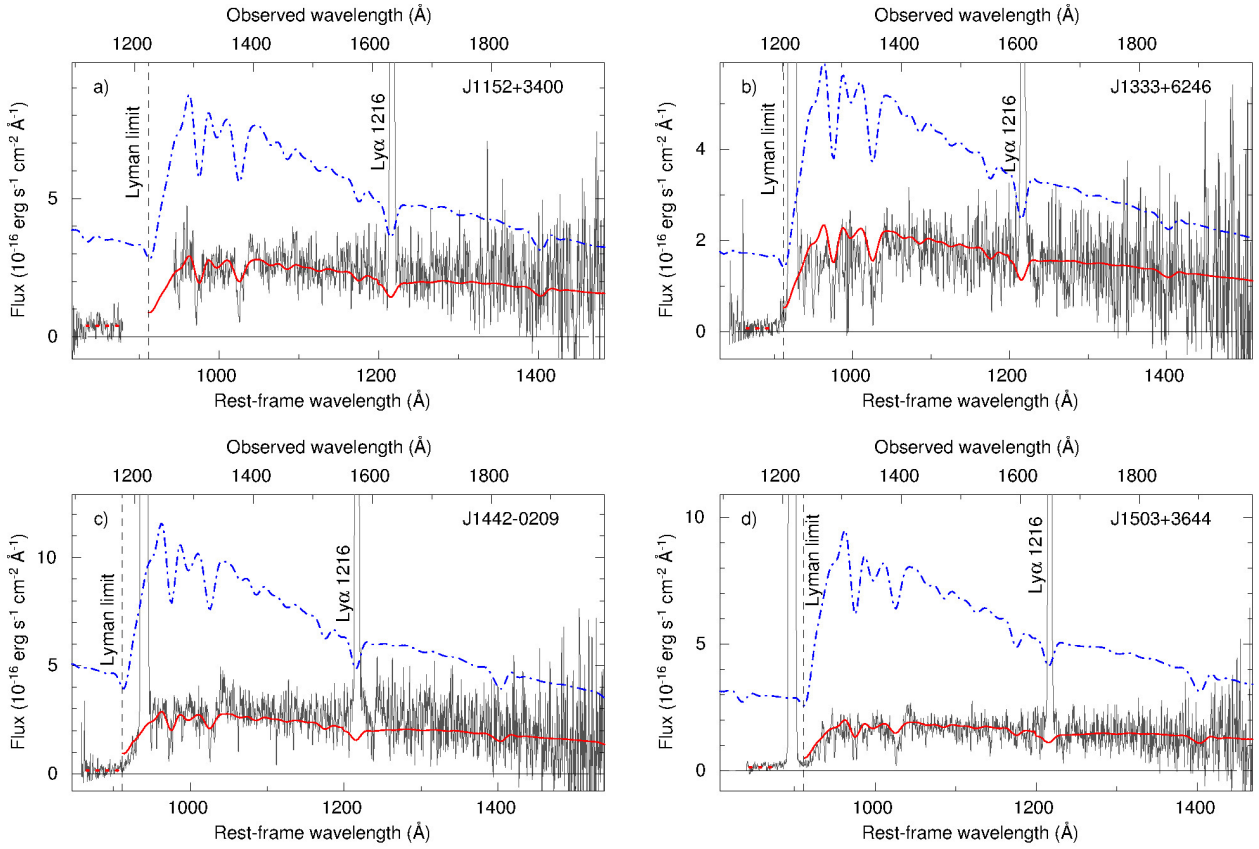

Figure 10. COS G140L spectra of our sources. On top of the observed spectra (grey lines) are superposed the modelled SEDs, reddened by both the Milky Way and internal extinctions (red solid lines). The unreddened SEDs are shown by the blue dash-dotted lines. Zero fluxes are represented by black solid horizontal lines.

Table 8. Parameters for the Hβ and Lyα emission lines

Name	$A(V)^{\rm a}_{\rm MW}$	$A(V)^{\rm a}_{\rm int}$	$A({\rm Ly}\alpha)^{\rm a}_{\rm MW}$	Hβ $F^{\rm b}$	Hβ EW$^{\rm c}$	Hβ $L^{\rm d}$	Lyα $F^{\rm b}$	Lyα EW$^{\rm c}$	Lyα $L^{\rm d}$	Lyα/H$\beta^{\rm e}$	$f_{\rm esc}({\rm Ly}\alpha)^{\rm f}$
J1152+3400	0.054	0.185	0.140	23.8	148	1.76	211.3	79	10.88	6.2	0.26
J1333+6246	0.052	0.152	0.135	9.8	147	0.62	137.1	75	5.56	9.0	0.39
J1442−0209	0.148	0.185	0.389	29.8	241	1.60	358.1	129	15.25	9.5	0.41
J1503+3644	0.041	0.283	0.106	19.2	219	1.70	178.3	98	9.15	5.4	0.22

[a]Extinction in mags. Data for J0925+1403 are presented in Izotov et al. (2016).
[b]Observed flux density in 10^{-16} erg s^{-1} cm^{-2}. Data for J0925+1403 are presented in Izotov et al. (2016).
[c]Rest-frame equivalent width in Å. EW(Lyα) for J0925+1403 is 83Å.
[d]Luminosity in 10^{42} erg s^{-1}. L(Hβ) is corrected for both the Milky Way and internal extinction, L(Lyα) is corrected only for the Milky Way extinction.
[e]Luminosity ratio. L(Lyα)/L(Hβ) for J0925+1403 is 5.5.
[f]$f_{\rm esc}$(Lyα) for J0925+1403 is 0.22.

9 LYMAN CONTINUUM DETECTION AND THE INFERRED ESCAPE FRACTION OF IONIZING PHOTONS

We now examine the COS spectra obtained with the G140L grating, primarily to examine the Lyman continuum of our sources, and inferences from these data.

9.1 Detection of Lyman continuum leakage

The observed G140L spectra are shown in Fig. 10 together with the predicted intrinsic SEDs obtained from fitting the observed optical SEDs (cf. below). The strong line at the observed wavelength of 1216Å, present in all objects except J1152+3400, is the residual of the geocoronal Lyα emission (not labelled), while the second brightest line labelled "Lyα 1216" is the Lyα line of the galaxy. The most striking finding is the detection of a non-zero flux in the Lyman continuum in all our sources. This is illustrated more clearly in Fig. 11,

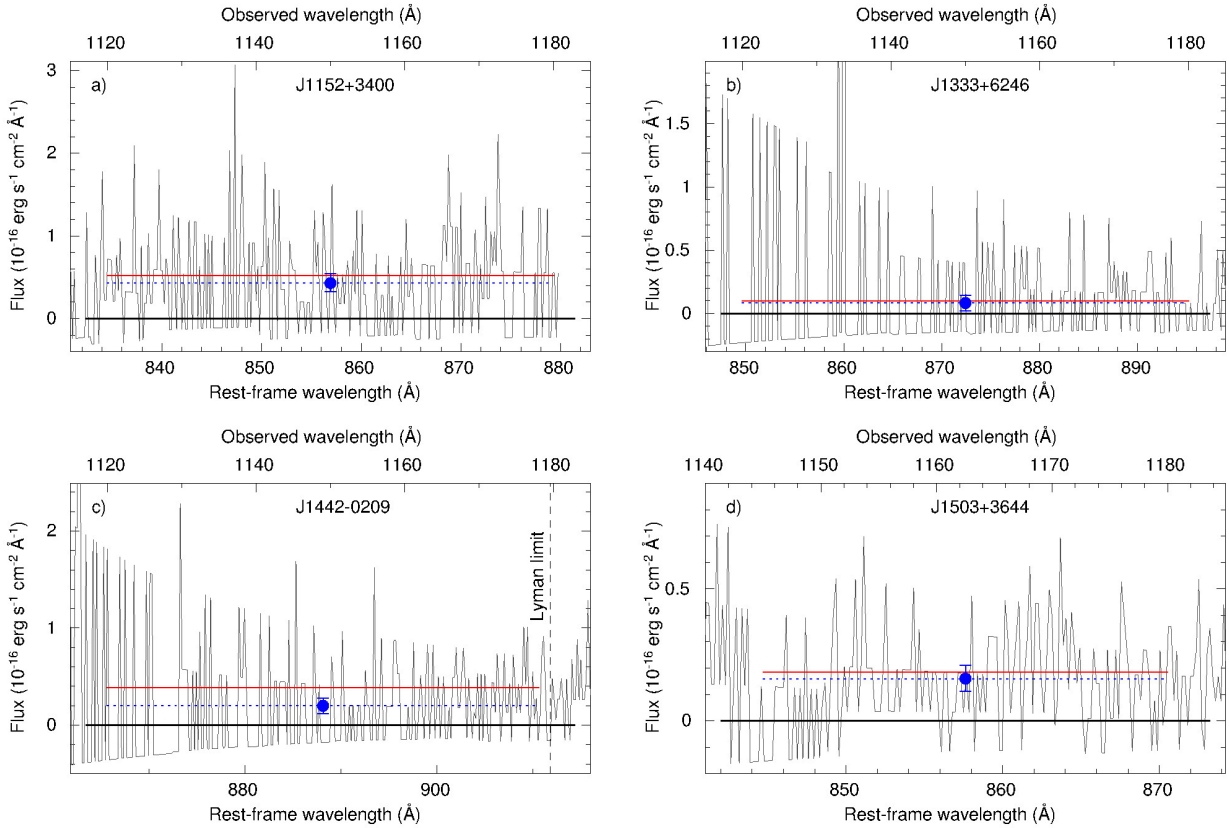

Figure 11. Expanded COS spectra showing the Lyman continuum. The average values with the 3σ error bars are shown by blue filled circles. The blue dotted horizontal lines indicate the observed mean LyC flux densities and the wavelength ranges used for averaging, while the red solid horizontal lines represent the LyC levels after correction for the Milky Way extinction. Zero fluxes are also shown by black horizontal lines.

which shows a blow-up of the LyC spectral region for all four galaxies. Similarly to J0925+1403 (Izotov et al. 2016) the important feature is that the Lyman continuum flux density for the rest-frame $\lambda < 912$Å is not zero, but positive, when averaged over the spectral range indicated by blue dotted and red solid horizontal lines. The lower cut on the wavelength range is typically due to declining sensitivity at the lowest wavelengths, but for J1503+3644 there is residual geocoronal N I 1134Å emission that needs to be avoided. The limit $\lambda < 1180$Å allows to avoid scattered geocoronal Lyα and/or wavelengths redward of 912Å in the rest frame of the galaxy. The floor at negative flux values is due to background subtraction (sometimes negative flux) and declining COS sensitivity. At the blue end one Poisson count corresponds to a larger "flux quantum", such that the negative floor is curved downward.

With fluxes in the range $(8 - 43) \times 10^{-18}$ erg s^{-1} cm^{-2} Å^{-1} the Lyman continuum is detected at the $> 10\sigma$ level in the J1152+3400 and J1503+3644 spectra, at the $\sim 8\sigma$ level in the J1442−0209 spectrum, and at the $\sim 5\sigma$ level in the J1333+6246 spectrum (Table 9). The observed mean levels of the LyC are indicated in Fig. 11 by blue dotted horizontal lines and blue filled circles. For comparison, the LyC detection of our first target, J0925+1403, is at the 11.8 σ level (Izotov et al. 2016).

The observed LyC emission should be corrected for extinction from the Milky Way before the determination of the LyC escape fraction. The average LyC flux densities corrected for the Milky Way extinction are shown in Fig. 11 by the red solid horizontal lines. The observed and corrected flux densities are reported in Table 9.

9.2 The Lyman continuum escape fraction

To derive the absolute escape fraction of Lyman continuum photons, $f_{\rm esc}$(LyC), we need to use the modelled flux $I(900)$ of the Lyman continuum emission at 900 Å, as produced by the massive stars, and compare it to the observed level (after correction for extinction in the Milky Way).

Two methods may be proposed to determine $I(900)$. The first method is based on "global" SED fits to the observed spectra and/or photometry, using evolutionary synthesis models, which then predict the intrinsic UV emission, both long- and short-ward of the Lyman limit. The second method relies on the fact that the intensities of hydrogen recombination lines are proportional to the number of ionizing photons emitted per unit time, N(Lyc). Both methods use the extinction-corrected flux $I_{\rm cor}(\rm H\beta)$ and rest-frame equivalent width EW(Hβ) of the Hβ emission line which are lower in LyC leaking galaxies because escaping ionizing radiation is not processed to produce nebular continuum and recombination line emission. Therefore, both methods should give accurate results if $f_{\rm esc}$(LyC) is much lower than unity. The advantage of the first method is that it takes into account

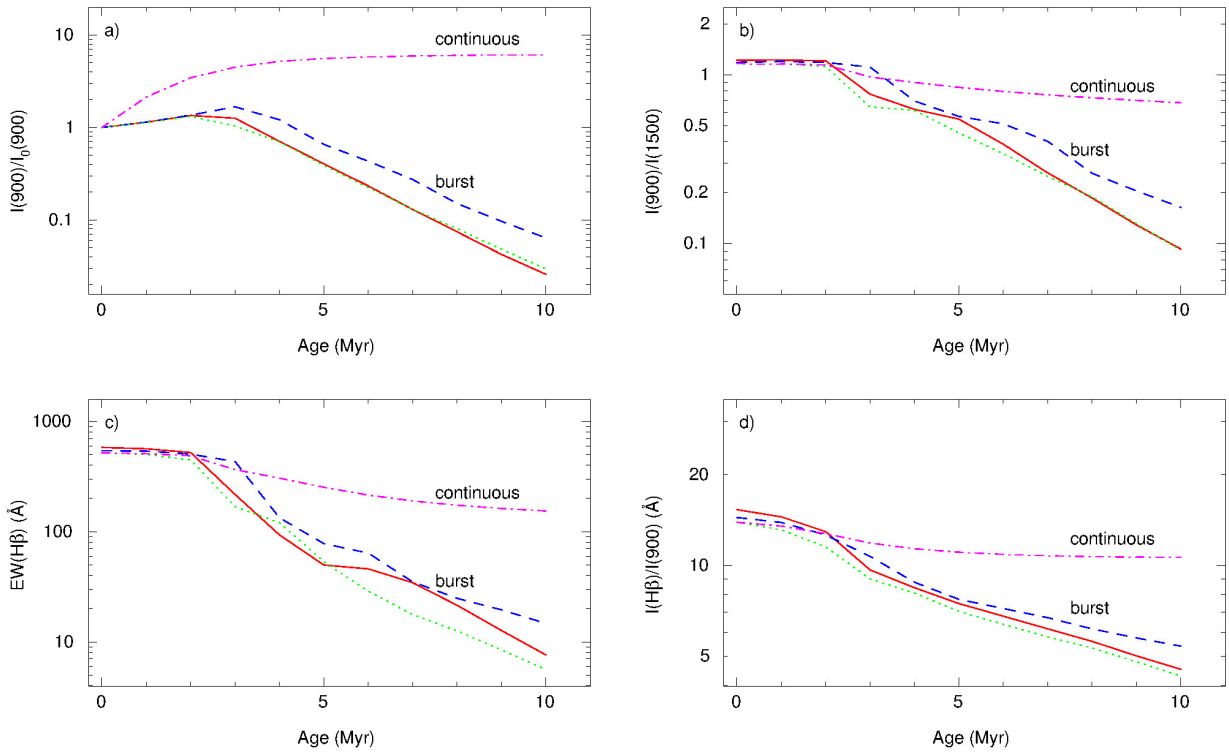

Figure 12. Dependence on the starburst age of: a) the flux at 900Å normalized to the initial flux, b) the flux ratio at wavelengths 900Å and 1500Å (in f_λ), c) the Hβ equivalent width EW(Hβ), and d) the Hβ-to-900Å flux ratio. Red solid lines and blue dashed lines are model predictions for instantaneous bursts with stars rotating with velocities 0 km s^{-1} and 400 km s^{-1}, respectively (Leitherer et al. 2014), green dotted lines are model predictions from Leitherer et al. (1999). Magenta dash-dotted lines are relations for continuous star formation with a constant SFR and models by Leitherer et al. (1999). For all calculations, a Salpeter (1955) IMF and stellar atmosphere models by Lejeune et al. (1997) and Schmutz et al. (1992) are adopted.

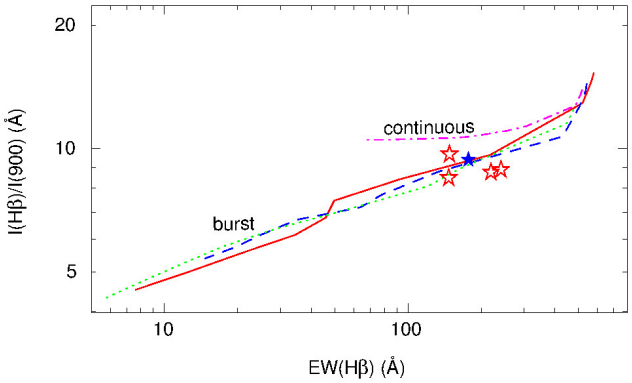

Figure 13. The dependence of the Hβ-to-900Å flux ratio on the Hβ equivalent width EW(Hβ) for instantaneous burst and continuous SFR models with negligible Lyman continuum escape. The meaning of lines is the same as in Fig. 12. The location of LyC leaking galaxies from Izotov et al. (2016) and this paper are shown by a blue filled star and red open stars, respectively.

the emission of the young and old stellar populations and thus potentially allows to derive more accurately the starburst age. On the other hand, the second method is simpler because no modelling is needed. However, it requires assumptions concerning the star formation history.

Concerning the first method, the modelled UV flux densities $I_{\rm mod}(\lambda)$ of young clusters with the ages obtained from SED fitting in the optical range are shown by the blue dash-dotted lines in Fig. 10. The reddened modelled UV SEDs are represented by the red solid lines. These SEDs are the same as the SEDs shown by red solid lines in Fig. 8. As discussed above (Sects. 5 and 7), we adopt for the reddening $R(V)_{\rm MW}$ = 3.1, $A(V)_{\rm MW}$ from the NED, $R(V)_{\rm int}$ = 2.4, $A(V)_{\rm int}$ as derived from the Balmer decrement after correction of the SDSS spectra for the Milky Way extinction. It is seen that the reddened SEDs reproduce very well the observed spectra (grey lines) for rest-frame wavelengths > 912Å.

The predicted flux densities $I_{\rm mod}(900)$ at 900 Å obtained from the best SED fits are listed in Table 9. To derive

Table 9. LyC escape fraction

Name	Monochromatic flux density[a] $I_{\rm mod}$[b] (900Å)	$I_{\rm mod}$[b] (1500Å)	$I_{\rm obs}$[c] (900Å)	$I_{\rm obs}$[c] (1500Å)	$I_{\rm esc}$[d] (900Å)	22μm/ 1500Å[e]	$f_{\rm esc}^{\rm rel}$[f] (LyC)	$f_{\rm esc}$[g] (LyC)	$f_{\rm esc}$[h] (LyC)	$f_{\rm esc}$[i] (LyC)
J0925+1403	4.40	5.84	$0.235^{+0.021}_{-0.020}$	1.55	$0.343^{+0.038}_{-0.037}$	1.08	0.236	0.072±0.008[j]	0.064	0.046
J1152+3400	3.30	3.14	$0.428^{+0.037}_{-0.034}$	1.36	$0.502^{+0.043}_{-0.040}$	...	0.335	0.132±0.011	0.132	0.116
J1333+6246	1.52	2.05	$0.083^{+0.023}_{-0.022}$	0.75	$0.090^{+0.025}_{-0.024}$	...	0.149	0.056±0.015	0.064	0.055
J1442−0209	4.59	3.99	$0.198^{+0.027}_{-0.028}$	1.50	$0.367^{+0.050}_{-0.052}$	1.44	0.154	0.074±0.010	0.090	0.032
J1503+3644	3.19	3.24	$0.160^{+0.018}_{-0.017}$	1.80	$0.195^{+0.021}_{-0.019}$	1.54	0.090	0.058±0.006	0.069	0.050

[a]in 10^{-16} erg s^{-1}cm^{-2}Å^{-1}.
[b]flux density derived from the modelled SED.
[c]observed flux density.
[d]observed flux density which is corrected for the Milky Way extinction.
[e]$\nu L_\nu(22\mu{\rm m})/[\nu L_{\nu,{\rm mod}}(1500) - \nu L_{\nu,{\rm obs}}(1500)]$.
[f]$I_{\rm mod}(1500)/I_{\rm obs}(1500)\times I_{\rm obs}(900)/I_{\rm mod}(900)$.
[g]$I_{\rm esc}(900)/[I_{\rm mod}(900)+I_{\rm esc}(900)]$, where $I_{\rm mod}(900)$ is derived from SED (first method).
[h]$I_{\rm esc}(900)/[I_{\rm mod}(900)+I_{\rm esc}(900)]$, where $I_{\rm mod}(900)$ is derived from Eq. 4 (second method).
[i]Derived from Eq. 5 (see also Leitet et al. 2013).
[j]This value is somewhat lower than the value $f_{\rm esc} = I_{\rm esc}(900)/I_{\rm mod}(900) = 0.078$ derived by Izotov et al. (2016).

the escape fraction $f_{\rm esc}$(LyC) we need to derive the total flux density produced by massive stars

$$I(900) = I_{\rm mod}(900) + I_{\rm esc}(900), \quad (2)$$

where $I_{\rm mod}(900)$ is the flux density of radiation producing the Hβ emission and $I_{\rm esc}(900)$ is the flux density of escaping radiation (Table 9). Then the escape fraction is obtained from

$$f_{\rm esc}({\rm LyC}) = \frac{I_{\rm esc}(900)}{I(900)} = \frac{I_{\rm esc}(900)}{I_{\rm mod}(900) + I_{\rm esc}(900)}. \quad (3)$$

Using Eq. 3 we derive escape fractions $f_{\rm esc}$(LyC) in the range between $\sim$ 6 % for J1333+6246 and J1503+3644, and 13 % for J1152+3400.

For the second method we need to consider the relation between N(LyC), which is directly related to the extinction-corrected flux density I(Hβ), and the flux density $I(900)$ at the reference wavelength representative of our LyC observations adopting a negligible LyC escape fraction. Since $N({\rm LyC}) \propto \int_0^{912} I(\lambda)/\lambda d\lambda$, and the shape of the ionizing spectrum $I(\lambda)$ depends e.g. on starburst age, the ratio I(Hβ)/$I(900)$ is not constant. However, it can be fairly accurately constrained, as we will now show. In Fig. 12 we examine how well the Hβ intensity traces the LyC flux $I(900)$ and how this depends on different IMFs, stellar atmospheres, and tracks. For a 1/10 solar metallicity, we plot how different quantities and their ratios which depend on the LyC flux, evolve with age of the burst stellar population. These relations were calculated with *Starburst99* models (Leitherer et al. 1999, 2014) adopting a Salpeter (1955) IMF, a combination of stellar atmosphere models by Lejeune et al. (1997) and Schmutz et al. (1992), and various Geneva evolutionary tracks for non-rotating and rotating stars. The LyC flux $I(900)$ produced during the first 3 Myr of the burst is nearly constant because the most massive stars with masses $\sim$ 100 M$_\odot$ are still on the main sequence and are producing ionizing radiation (Fig. 12a). Later, between 3 and 10 Myr, the LyC flux rapidly decreases, by a factor of $\sim$ 30. Similarly, $I(900)/I(1500)$ and EW(Hβ) decrease by a factor $\sim$10 and $\sim$30, respectively, during the same time period (Fig. 12b and 12c). On the other hand, the I(Hβ)/$I(900)$ ratio diminishes only by a factor $\sim$ 3 (Fig. 12d), and is consistent with the Izotov et al. (2016) relation for younger ages. The decrease of I(Hβ)/$I(900)$ is explained by the evolution of the shape of the ionizing spectrum with time. By contrast, the relations in Fig. 12 for continuous star formation with a constant SFR converge asymptotically toward constant values after an age of $\sim$ 5 Myr.

To determine the flux density $I(900) = I_{\rm mod}(900) + I_{\rm esc}(900)$, it is more convenient to use relations between the I(Hβ)/$I(900)$ ratio and EW(Hβ), since both the Hβ flux and the Hβ equivalent width can directly be derived from observations. These relations for instantaneous bursts and different sets of stellar atmosphere models are shown in Fig. 13 (labelled "burst"), and can be approximated as

$$\frac{I_{\rm cor}({\rm H}\beta)}{I_{\rm mod}(900)} \approx \frac{I({\rm H}\beta)}{I(900)} = 2.99 \times {\rm EW}({\rm H}\beta)^{0.228} \ \ {\rm Å} \quad (4)$$

for a negligible LyC escape fraction, where EW(Hβ) is in Å. As can be seen, this relation is fairly weakly model-dependent, which allows us to determine quite accurately the flux $I_{\rm mod}(900)$ (within $\leqslant$ 10%) adopting the rest-frame equivalent width EW(Hβ) from Table 8 and the extinction-corrected Hβ flux $I_{\rm cor}$(Hβ) from Table 5. The characteristic value $I_{\rm cor}({\rm H}\beta)/I_{\rm mod}(900)$ for our galaxies (shown by stars) is $\sim$8–10. For continuous star formation with a constant SFR, the ratio attains the asymptotic value of $\sim$ 11 (labelled "continuous" in Fig. 13). We note that, in general, EW(Hβ) in galaxies is not only determined by the recent starburst, but also by the radiation of older stellar populations in the optical range. But for our galaxies, EW(Hβ) is mainly set by the young stellar population. Otherwise, the intrinsic EW(Hβ) to be compared to the models in Fig. 13 would be even higher. However, our adopted value of $I_{\rm cor}({\rm H}\beta)/I_{\rm mod}(900)$ would not change much.

The escape fraction with the second method is derived from Eq. 3 (similar to the first method), but with $I_{\rm mod}(900)$ obtained from Eq. 4 and adopting a Salpeter IMF (Salpeter 1955), Geneva evolutionary tracks (Meynet et al. 1994) of non-rotating stars and a combination of stellar atmosphere

models (Lejeune et al. 1997; Schmutz et al. 1992). It ranges from ~ 6 % to ~ 13 % (Table 9) with the errors, which are similar to those given in Table 9 for method 1.

These values agree within the errors with the values from the first method based on SED fitting (cf. above). We decided to adopt the $f_{\rm esc}$ derived by method 1, as the values derived by method 2, not based on modelling of the SEDs, are more approximate.

The $f_{\rm esc}$(LyC) values, derived by either method, are higher than the $f_{\rm esc}$(LyC) of the other four low-redshift galaxies with known LyC leakage.

In the literature, the LyC escape fraction is often estimated from the equation (Leitet et al. 2013)

$$f_{\rm esc}({\rm LyC}) = f_{\rm esc}^{\rm rel}({\rm LyC}) \times 10^{-0.4\times A(1500)}, \quad (5)$$

where

$$f_{\rm esc}^{\rm rel}({\rm LyC}) = \frac{[I(1500)/I(900)]_{\rm mod}}{[I(1500)/I(900)]_{\rm obs}}, \quad (6)$$

$I(900)$ and $I(1500)$ are the flux densities at rest-frame wavelengths 900Å and 1500Å, respectively, and the subscripts "mod" and "obs" denote modelled and observed flux densities. The values of the relative escape fraction $f_{\rm esc}^{\rm rel}$(LyC) for our objects, derived from SED fitting and listed in Table 9, are between 9 and 33 %. The use of Eq. 5 would result in an underestimate of $f_{\rm esc}$(LyC) for two reasons: 1) Eq. 5 does not take into account the fact that the extinction at 900Å though uncertain is expected to be higher than at 1500Å (Mathis 1990); and 2) the observed flux density $I_{\rm obs}(900)$ is not corrected for foreground extinction from the Milky Way as it should. Indeed, using $I_{\rm mod}$, $I_{\rm obs}$ and $10^{-0.4\times A(1500)} \equiv I_{\rm obs}(1500)/I_{\rm mod}(1500)$ we find that, depending on the object, the $f_{\rm esc}$(LyC) derived from Eq. 5 is up to 55 % lower than the value obtained from SED fitting (last column in Table 9).

In the above determination of $f_{\rm esc}$(LyC) by different methods, the UV attenuation is determined from the Balmer decrement and an analysis of the observed SED from the UV to the optical domains. In other words, it assumes that the young star-forming population emitting the UV and Lyman continuum can be wholly accounted for in this manner. This method should be correct if our sources do not contain highly dust-obscured star-forming regions which are invisible in the UV-to-optical range. The sky regions where our galaxies are located have been observed in the mid-infrared range by *Wide-field Infrared Survey Explorer* (*WISE*). Data for all these galaxies but one are present in the AllWISE Source Catalog[8]. Only the galaxy J0925+1403 appears in the list of rejected objects. The *WISE* magnitudes of the four studied galaxies are given in Table 2. The *WISE* colours of our galaxies do not resemble those of the most nearby star-forming galaxies which have a major contribution from stellar emission in the $W1$ and $W2$ bands and are characterized by $W1-W2 < 0.5$ mag. Instead, the red $W1-W2 > 1$ of our objects imply a considerable contribution of the warm and hot dust to their mid-infrared luminosity (Izotov et al. 2014a).

Three out of five galaxies were detected by *WISE* in the $W4$ band at 22μm. The estimated ratio of the 22μm luminosity, which is a characteristic of warm dust, to the luminosity absorbed at 1500Å in these galaxies is of order of unity (Table 9). As the luminosity of the cold dust emitting in the far-infrared range of extreme starbursts (not accessible to *WISE*) is less or comparable to the luminosity of the warm dust (Izotov et al. 2014b), we conclude that the UV luminosity absorbed in visible star-forming regions of our galaxies is consistent with the luminosity emitted by dust in the infrared range. Optical, near- and mid-infrared observations of other low-metallicity SFGs with similar properties suggest that they are relatively transparent (Izotov & Thuan 2011, 2016). That there is not much dust-obscured hidden star formation is also implied by the observed thermal free-free cm radio emission in dwarf galaxies with optical and infrared observations. Its flux density is consistent with the value derived from the flux density of the Hβ emission line (Izotov et al. 2014b), indicating that there is not a considerable amount of additional star formation, not seen in the UV range, in our galaxies.

10 DISCUSSION

To the best of our knowledge, our experiment is the first where compact star-forming galaxies with strong emission lines and high [O III]λ5007/[O II]λ3727 ratios are observed in the Lyman continuum. Furthermore, the entire sample (5 out of 5) at $z \sim 0.3$ is found to emit Lyman continuum radiation, with absolute escape fractions ranging between 6 % and 13 %. Our observations thus significantly expand the sample of Lyman continuum leakers at low redshift, from four previously known galaxies (Leitet et al. 2013; Borthakur et al. 2014; Leitherer et al. 2016) to nine. The newly discovered sources also show significantly higher LyC escape fractions, compared to $f_{\rm esc}({\rm LyC}) \approx (1-4.5)$ % previously found.

Apparently, the selection criteria we adopted are very efficient in finding LyC leakers. As such, this finding is probably one of the most important results of our study.

Compactness and a peculiar emission line ratio as selection criteria, were previously already suggested to be related to Lyman continuum leakage. Jaskot & Oey (2013) and Nakajima & Ouchi (2014) have proposed that extreme [O III]λ5007/[O II]λ3727 ratios may be due to high escape fractions of ionizing photons and have argued that this could be the case for some "Green Pea" galaxies at $z \sim 0.1-0.3$ or in $z \sim 2-3$ LAEs. For comparison, Heckman et al. (2011) examined so-called Lyman-break analogs (LBAs) and suggested that a subset of them, those with a compact massive ($\sim 10^9$ M$_\odot$) dominant central object, could be LyC leakers. The LBAs have lower excitation and higher masses compared to our galaxies. The leaking galaxy J0921+4509, recently found by Borthakur et al. (2014) is currently the only LBA for which escaping Lyman continuum radiation has been found at the low level of ~ 1 %. However, the [O III]λ5007/[O II]λ3727 ratio in this galaxy of ~ 0.3 is much lower than that for the GPs in our sample.

In Fig. 14 we present the relation between $f_{\rm esc}$(LyC) and O_{32} for known low-redshift LyC leaking galaxies. It shows a trend of increasing $f_{\rm esc}$(LyC) with increasing O_{32}, implying that compact low-mass SFGs with high [O III]λ5007/[O II]λ3727 ratios may lose a considerable fraction of their LyC emission to the IGM. The correlation in

[8] http://irsa.ipac.caltech.edu/Missions/wise.html.

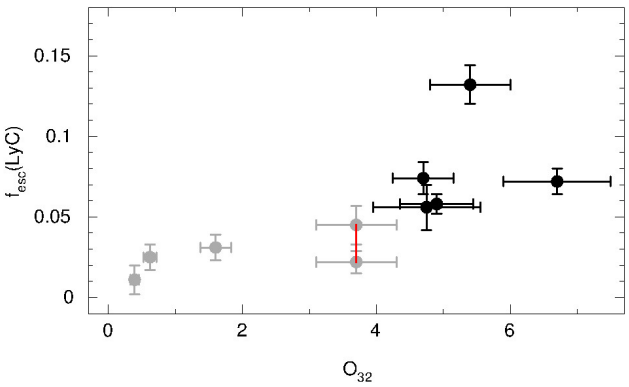

Figure 14. Relation between the Lyman continuum escape fraction $f_{\rm esc}$(LyC) and the [O III]λ5007/[O II]λ3727 emission-line ratio in low-redshift LyC leaking galaxies. GP galaxies from Izotov et al. (2016) and this paper are shown by black symbols, while the galaxies from Leitet et al. (2013), Borthakur et al. (2014) and Leitherer et al. (2016) are represented by grey symbols. Two different measurements of $f_{\rm esc}$(LyC) in Tol 1247−232 are connected by the red line.

Figure 14 suggests that the high O_{32} criterion plays an important role: it selects out low-metallicity and hence low-mass galaxies. Our observations (Izotov et al. 2016, and this paper) are the first reported LyC observations – and successful detections – of "Green Pea" galaxies, which are a subset of a wider category called luminous compact galaxies (LCGs) by Izotov et al. (2011).

At high redshifts, searches for Lyman continuum leakers have been very difficult, and numerous candidates have not withstood careful examination (see Introduction and references therein). In particular, most candidates have turned out to be due to chance alignments with foreground objects, as revealed by *HST* imaging (cf. Vanzella et al. 2010b, 2012). Currently the most robust high-redshift Lyman continuum leaking galaxy is arguably *Ion2* at $z = 3.2$ (Vanzella et al. 2015; de Barros et al. 2016). Interestingly, this galaxy shares many properties with the sources found here (cf. Schaerer et al., in preparation). In particular, follow-up observations of *Ion2* – found from imaging in the Lyman continuum – have shown a high ratio $O_{32} > 10$, again in line with the criterion used to select our targets.

The available data, at high- and low-z, and our successful new *HST* observations thus all concur to indicate that compactness and high O_{32} are promising criteria to identify Lyman continuum leakers. However, we note that these conditions are necessary but not sufficient for selecting galaxies with strong Lyα emission line and escaping LyC emission. For example, the nearby BCD SBS 0335–052E is characterised by a high $O_{32} \sim 10$, but its Lyα line is in absorption (Thuan & Izotov 1997). The LyC flux in its *FUSE* spectrum is very low (Thuan, Lecavelier des Etangs & Izotov 2005), although the data are not of high quality. Clearly, larger statistics are needed to verify how good criteria of compactness and high O_{32} are for selecting LyC leaking galaxies. In particular, future observations and further exploration will show how the escape fraction varies with [O III]λ5007/[O II]λ3727 ratio, and how it depends on the physical parameters of the galaxies.

Although successful in finding Lyman continuum leaking galaxies, our selection criteria as such do not yet explain the *physical cause* of the observed escape of ionizing photons. Compactness, or more precisely a high star formation rate surface density, Σ, inducing a strong feedback, rapid outflow etc., may physically be related to leakage of Lyman continuum radiation, as suggested e.g. by Heckman et al. (2011) and Borthakur et al. (2014), and explored further by Sharma et al. (2016). As shown previously in Fig. 7, our sources have a very large Σ both compared to low- and high-redshift sources. Whether they also show strong/efficient outflows capable of carving out channels in the ISM or blowing it (partly) away, remains to be seen. Further analysis, such as that of the interstellar absorption lines may shed light on this issue.

11 CONCLUSIONS

In this paper we present new *Hubble Space Telescope* (*HST*) Cosmic Origins Spectrograph (COS) observations of four sources in our sample of five compact star-forming galaxies (SFGs) with high O_{32} = [O III]λ5007/[O II]λ3727 flux ratios $\gtrsim 5$ at redshifts $z \sim 0.3$, aiming to study Lyα emission and escaping Lyman continuum (LyC) radiation. The first observations of our sample, showing a clear leakage of LyC radiation in one galaxy, have been reported in Izotov et al. (2016). Our main results are as follows:

1. Escaping LyC radiation is detected in all five galaxies. We derive absolute escape fractions $f_{\rm esc}$(LyC) in the range of ~ 6 % – 13 %, the highest values found so far in low-redshift SFGs.

2. A double-peaked Lyα emission line, with a small separation between the blue and red peaks, is detected in the spectra of all galaxies, as suggested by Verhamme et al. (2015) for LyC leaking galaxies. The luminosities and rest-frame equivalent widths of the Lyα emission line are among the highest found so far for Lyα emitters (LAEs) at any redshift. We obtain escape fractions $f_{\rm esc}$(Lyα) ~ 20 % – 40 %, also among the highest known for LAEs.

3. The COS/NUV acquisition images reveal bright star-forming regions in the centers of galaxies and an exponential disc at the outskirts with a disc scale length in the range $\sim$ 0.6 – 1.4 kpc, indicating that the galaxies are dwarf disc systems.

4. All five galaxies are characterized by high star-formation rates SFR $\sim 14 - 50$ M$_\odot$ yr^{-1}. They have high

SFR densities $\Sigma \sim 2-35\ M_\odot\ \mathrm{yr}^{-1}\mathrm{kpc}^{-2}$, among the highest known so far for star-forming galaxies at any redshift. Their stellar masses $M_\star$ are in the range $\sim (0.2-4)\times 10^9$ $M_\odot$. Their metallicities, accurately determined from the optical emission lines are in the range $12+\log(\mathrm{O/H}) = 7.8-8.0$, or $\sim 1/8-1/5$ solar. These properties are comparable to those of high-redshift star-forming galaxies, such as LAEs.

5. From modelling of the UV-to-optical SEDs we constrained the extinction law. We find that SEDs reddened with extinction curves by Cardelli et al. (1989) fit best the observed COS UV spectra if the selective extinction $R(V)=A(V)/E(B-V) \approx 2.4-2.7$ for the internal galaxy extinction is lower than the canonical value of 3.1 and the empirical value of 4.05 ± 0.80 for starburst galaxies by Calzetti et al. (1994). This finding is consistent with the data for the Small Magellanic Cloud with a similar metallicity.

6. The observations demonstrate that a selection for compact high-excitation star-forming galaxies showing a high ratio of [O III]λ5007/[O II]λ3727, thus combining various criteria suggested in the literature (cf. Heckman et al. 2011; Jaskot & Oey 2013; Nakajima & Ouchi 2014), appears to pick up very efficiently sources with escaping Lyman continuum emission. Our results should open new and more effective ways to find and explore the sources of cosmic reionization in the near future.

ACKNOWLEDGEMENTS

We thank H. Yang for valuable comments. Based on observations made with the NASA/ESA *Hubble Space Telescope*, obtained from the data archive at the Space Telescope Science Institute. STScI is operated by the Association of Universities for Research in Astronomy, Inc. under NASA contract NAS 5-26555. Support for this work was provided by NASA through grant number HST-GO-13744.001-A from the Space Telescope Science Institute, which is operated by AURA, Inc., under NASA contract NAS 5-26555. I.O. acknowledges a grant GACR 14-20666P of the Czech National Foundation. Funding for the SDSS and SDSS-II was provided by the Alfred P. Sloan Foundation, the Participating Institutions, the National Science Foundation, the U.S. Department of Energy, the National Aeronautics and Space Administration, the Japanese Monbukagakusho, the Max Planck Society, and the Higher Education Funding Council for England. The SDSS was managed by the Astrophysical Research Consortium for the Participating Institutions. Funding for SDSS-III has been provided by the Alfred P. Sloan Foundation, the Participating Institutions, the National Science Foundation, and the U.S. Department of Energy Office of Science. The SDSS-III web site is http://www.sdss3.org/. SDSS-III is managed by the Astrophysical Research Consortium for the Participating Institutions of the SDSS-III Collaboration. GALEX is a NASA mission managed by the Jet Propulsion Laboratory. This research has made use of the NASA/IPAC Extragalactic Database (NED) which is operated by the Jet Propulsion Laboratory, California Institute of Technology, under contract with the National Aeronautics and Space Administration. This publication makes use of data products from the Wide-field Infrared Survey Explorer, which is a joint project of the University of California, Los Angeles, and the Jet Propulsion Laboratory/California Institute of Technology, funded by the National Aeronautics and Space Administration.

REFERENCES

Ade P. A. R. et al., 2014, A&A, 571, A16
Ahn C. P. et al., 2014, ApJS, 211, 17
Asplund M., Grevesse N., Sauval A. J., Scott P., 2009, Ann.Rev.Astron.Astrophys., 47, 481
Baldwin J. A., Phillips M. M., Terlevich R., 1981, PASP, 93, 5
Borthakur S., Heckman T. M., Leitherer C., Overzier R. A., 2014, Science, 346, 216
Bouchet P., Lequeux J., Maurice E., Prévot L., Prévot-Burnichon M. L., 1985, A&A, 149, 330
Boutsia K. et al., 2011, ApJ, 736, 41
Bouwens R. J., Illingworth G. D., Oesch P. A., Caruana J., Holwerda B., Smit R., Wilkins S., 2015a, ApJ, 811, 140
Bouwens R. J., Smit R., Labbe I., Franx M., Caruana J., Oesch P., Stefanon M., Rasappu N., 2015b, ApJ, in press; preprint arXiv:1511.08504
Brisbin D., Harwit M., 2012, ApJ, 750, 142
Calzetti D., Kinney A. L., Storchi-Bergmann T., 1994, ApJ, 429, 582
Calzetti D., Armus L., Bohlin R. C., Kinney A. L., Koornneef J., Storchi-Bergmann T., 2000, ApJ, 533, 682
Cardamone C. et al., 2009, MNRAS, 399, 1191
Cardelli J. A., Clayton G. C., Mathis J. S., 1989, ApJ, 345, 245
Cowie L. L., Barger A. J., Trouille L., 2009, ApJ, 692, 1476
Curtis-Lake E. et al., 2016, MNRAS, 457, 440
de Barros S. et al., 2016, A&A, 585, A51
Deharveng J.-M., Buat V., Le Brun V., Milliard B., Kunth D., Shull J. M., Gry C., 2001, A&A, 375, 805
Dressler A., Henry A., Martin C. L., Sawicki M., McCarthy P., Villaneuva E., 2015, ApJ, 806, 19
Fathi K., Allen M., Boch T., Hatziminaoglou E., Peletier R. F., 2010, MNRAS, 406, 1595
Fechner C., Reimers D., 2007, A&A, 461, 847
Finkelstein S. L. et al., 2012, ApJ, 758, 93
Finkelstein S. L., et al., 2015, ApJ, 810, 71
Fontanot F., Cristiani S., Vanzella E., 2012, MNRAS, 425, 1413
Giallongo, E. et al., 2015, A&A, 578, A83
Gnedin N. Y., Kravtsov A. V., Chen H.-W., 2008, ApJ, 672, 765
Gordon K. D., Clayton G. C., 1998, ApJ, 500, 816
Gordon K. D., Clayton G. C., Misselt K. A., Landolt A. U., Wolff M. J., 2003, ApJ, 594, 279
Grazian A. et al., 2016, A&A, 585, A48
Green J. C. et al., 2012, ApJ, 744, 60
Grimes, J. P. et al., 2009, ApJ, 181, 272
Guseva N. G., Izotov Y. I., Papaderos P., Fricke K. J., 2007, A&A, 464, 885
Haardt F., Madau P., 2012, ApJ, 746, 125
Hayes M., 2015, PASA, 32, e027
Hayes M. et al., 2014, ApJ, 782, 6
Heckman T. M. et al., 2011, ApJ, 730, 5
Henry A., Scarlata C., Martin C. S., Erb D., 2015, ApJ, 809, 19

Hummer D. G., Storey P. J., 1987, MNRAS, 224, 801
Inoue A. K., Shimizu I., Iwata I., Tanaka M., 2014, MNRAS, 442, 1805
Iwata I. et al., 2009, ApJ, 692, 1287
Izotov Y. I., Thuan T. X., 2011, ApJ, 734, 82
Izotov Y. I., Thuan T. X., 2016, MNRAS, 457, 64
Izotov Y. I., Thuan T. X., Lipovetsky V. A., 1994, ApJ, 435, 647
Izotov Y. I., Stasińska G., Meynet G., Guseva N. G., Thuan T. X., 2006, A&A, 448, 955
Izotov Y. I., Guseva N. G., Thuan T. X., 2011, ApJ, 728, 161
Izotov Y. I., Guseva N. G., Fricke K. J., Henkel C., 2014a, A&A, 561, A33
Izotov Y. I., Guseva N. G., Fricke K. J., Krügel E., Henkel C., 2014b, A&A, 570, A97
Izotov Y. I., Guseva N. G., Fricke K. J., Henkel C., 2015, MNRAS, 451, 2251
Izotov Y. I., Orlitová I., Schaerer D., Thuan T. X., Verhamme A., Guseva N. G., Worseck G., 2016, Nature, 529, 178
Jaskot A. E., Oey M. S., 2013, ApJ, 766, 91
Kauffmann G. et al., 2003, MNRAS, 341, 33
Kennicutt R. C., Jr., 1998, Ann.Rev.Astron.Astrophys., 36, 189
Khaire V., Srianand R., Choudhury T. R., Gaikwad P., 2016, MNRAS, 457, 4051
Kimm T., Cen R., 2014, ApJ, 788, 121
Lehnert M. D., Heckman T. M., 1996, ApJ, 472, 546
Leitet E., Bergvall N., Hayes M., Linné S., Zackrisson E., 2013, A&A, 553, A106
Leitherer C., 1990, ApJS, 73, 1
Leitherer C., Ferguson H. C., Heckman T. M., Lowenthal J. D., 1995, ApJ, 454, L19
Leitherer C. et al., 1999, ApJS, 123, 3
Leitherer C., Ekström S., Meynet G., Schaerer D., Agienko K. B., Levesque E. M., 2014, ApJS, 212, 14
Leitherer C., Hernandez S., Lee J. C., Oey M. S., 2016, ApJ, in press; preprint arXiv:1603.06779
Lejeune T., Buser R., Cuisinier F., 1997, A&AS, 125, 229
Ma X., Kasen D., Hopkins P. F., Faucher-Giguére C.-A., Quataert E., Kereš D., Murray N., 2015, MNRAS, 453, 960
Madau P., Haardt F., 2015, ApJL, 813, L8
Mathis J. S., 1990, Ann.Rev.Astron.Astrophys., 28, 10
Meynet G., Maeder A., Schaller G., Schaerer D., Charbonnel C., 1994, A&AS, 103, 97
Mitra S., Ferrara A., Choudhury T. R., 2013, MNRAS, 428, L1
Mostardi R. E., Shapley A. E., Nestor D. B., Steidel C. C., Reddy N. A., Trainor R. F., 2013, ApJ, 779, 65
Mostardi R. E., Shapley A. E., Steidel C. C., Trainor R. F., Reddy N. A., Siana B., 2015, ApJ, 810, 107
Murthy J., 2014, ApJS, 213, 32
Nakajima K., Ouchi M., 2014, MNRAS, 442, 900
Nestor D. B., Shapley A. E., Steidel C. C., Siana B., 2011, ApJ, 736, 18
Östlin G. et al., 2014, ApJ, 797, 11
Ouchi M. et al., 2009, ApJ, 706, 1136
Paardekooper J.-P., Khochfar S., Dalla Vecchia C., 2015, MNRAS, 451, 2544
Papaderos P., Izotov Y. I., Thuan T. X., Noeske K. G., Fricke K. J., Guseva N. G., Green R. F., 2002, A&A, 393, 461
Razoumov A. O., Sommer-Larsen J., 2010, ApJ, 710, 1239
Robertson B. E. et al., 2013, ApJ, 768, 71
Robertson B. E., Ellis R. S., Furlanetto S. R., Dunlop J. S., 2015, ApJL, 802, L19
Rutkowski M. G. et al., 2016, ApJ, 819, 81
Salpeter E. E., 1955, ApJ, 121, 161
Sandberg A., Östlin G., Melinder J., Bik A., Guaita L., 2015, ApJ, 814, L10
Schmutz W., Leitherer C., Gruenwald, R., 1992, PASP, 104, 1164
Sharma M., Theuns T., Frenk C., Bower R., Crain R., Schaller M., Schaye J., 2016, MNRAS, 458, L94
Shull J. M., France K., Danforth C. W., Smith B., Tumlinson J., 2010, ApJ, 722, 1312
Siana B. et al., 2015, ApJ, 804, 17
Stasińska G., Izotov Y., Morisset C., Guseva N., 2015, A&A, 576, A83
Steidel C. C., Pettini M., Adelberger K. L., 2011, ApJ, 546, 665
Storey P. J., Hummer D. G., 1995, MNRAS, 272, 41
Syphers D., Anderson S. F., Zheng W., Meiksin A., Schneider D. P., York D. G., 2012, AJ, 143, 100
Thuan T. X., Izotov Y. I., 1997, ApJ, 477, 661
Thuan T. X., Lecavelier des Etangs A., Izotov Y. I., 2005, ApJ, 621, 269
Trebitsch M., Blaizot J., Rosdahl J., 2015, SF2A-2015: Proceedings of the Annual meeting of the French Society of Astronomy and Astrophysics. Eds.: F. Martins, S. Boissier, V. Buat, L. Cambrésy, P. Petit, pp.105-108, 105
Vanzella E. et al., 2010a, ApJ, 725, 1011
Vanzella E., Siana B., Cristiani S., Nonino M., 2010b, MNRAS, 404, 1672
Vanzella E. et al., 2012, ApJ, 751, 70
Vanzella E. et al., 2015, A&A, 576, A116
Verhamme A., Orlitová I., Schaerer D., Hayes M., 2015, A&A, 578, A7
Wise J. H., Cen R., 2009, ApJ, 693, 984
Wise J. H., Demchenko V. G., Halicek M. T., Norman M. L., Turk M. J., Abel T., Smith B. D., 2014, MNRAS, 442, 2560
Worseck G. et al., 2011, ApJ, 733, L24
Wright E. L., 2006, PASP, 118, 1711
Yajima H., Choi J.-H., Nagamine K., 2011, MNRAS, 412, 411
Yajima H., Li Y., Zhu Q., Abel T., Gronwall C., Ciardullo R., 2014, MNRAS, 440, 776
Yang H. Malhotra S., Gronke M., Rhoads J. E., Dijkstra M., Jaskot A., Zheng Z., Wang J., 2016, ApJ, 820, 130

This paper has been typeset from a TEX/ LATEX file prepared by the author.